Energy Conversion and Management 268 (2022) 115996

Contents lists available at ScienceDirect

Energy Conversion and Management

journal homepage: www.elsevier.com/locate/enconman

Exergoeconomic analysis and optimization of a high-efficient multi-generation system powered by Sabalan (Savalan) geothermal power plant including branched GAX cycle and electrolyzer unit

Miryasin Seiiedhoseiny [a], Leyla Khani [a], Mousa Mohammadpourfard [a,b,*], Gülden G. Akkurt [b]

[a] Faculty of Chemical and Petroleum Engineering, University of Tabriz, Tabriz, Iran
[b] Department of Energy Systems Engineering, Izmir Institute of Technology, Izmir, Turkey

ARTICLE INFO

Keywords:
Branched GAX cycle
Geothermal energy
Multi-generation
Exergoeconomic
Two-objective optimization

ABSTRACT

Employing suitable subsystems to reach high efficiency and low cost in renewable-based power plants is more crucial. The geothermal energy heat source is located in many countries, but this has never been investigated to run a multi-generation system, including a branched GAX cycle and an electrolyzer. In this path, a high-efficient multi-generation system powered by a Sabalan (Savalan) geothermal power plant consisting of a single flash cycle, a branched GAX cycle, and an electrolyzer is presented and scrutinized from thermodynamic and exergoeconomic viewpoints. In the end, a two-objective optimization, by using the Total Unit Cost of Product (TUCP) and energy efficiency as objectives, is utilized to find the optimum operating conditions. Critiques and studies of variables reveal that the produced hydrogen rate remains unchanged at 5.655 kg/h by changing the degassing value and temperature of the generator, condenser 2, and evaporator. By increasing the flash tank pressure from 5.2 bar to 7 bar, the cooling and heating loads rise about 108.4%, while the net electricity falls from 3977 kW to 3506 kW. Interestingly, the TUCP has a minimum value at the evaporator temperature of 273 K and condenser 2 temperature of 322.3 K. The optimization results indicate the values of the produced hydrogen rate and net electricity with 5.85 kg/h and 4187 kW are more than those of the base case. Also, the optimal values are 7.046 $/GJ, 36.82%, and 65.42% for the TUCP and energy and exergy efficiencies, respectively.

1. Introduction

Nowadays, with increasing energy consumption due to population growth and industrial development, the world is facing the problem of running out of available fossil fuels [1,2]. Therefore, to deal with such a problem, researchers and designers have been obliged to use renewable energies [3,4]. The burn of fossil fuels results in environmental damage, including Greenhouse Gas (GHG) emissions, climate change, and global warming. Renewable energies such as solar, wind, fuel cell, biomass, and geothermal are desirable alternatives to fossil fuels, which can be used in various applications such as generating cold, heat, electricity, fresh water, and hydrogen [5–8]. Therefore, the development of geothermal energy can drastically decrease energy consumption and the negative environmental consequences of fossil fuels. There are a lot of geothermal springs wherever volcanoes are active, especially in the United States and China [9]. Geothermal energy is one of the well-established resources for thermodynamic systems. Also, Japan is one of the countries which has focused on utilizing geothermal energy. Experts believe that by 2050, 10% of energy demand will be met using geothermal energy, which is comparable to the current value of 0.2% [10].

The typical temperature range of geothermal energy sources is 30-220 °C. It is important to note that as a geothermal source is used more frequently, its available temperature is decreases [11]. Hence, the goal of next-generation geothermal systems is to use low-temperature resources. Geothermal energy sources are classified based on geothermal production well temperature [12]. High-temperature sources have temperatures above 150 °C, while medium-temperature sources work in the temperature range of 90-150 °C, and below 90 °C are known as low-temperature sources. In most geothermal sources across the world, the outflow water is liquid. However, it can also be in the superheated and/or saturated states [12]. Using underground water to generate power and heat is the common method to utilize geothermal energy, specifically in cold regions. In addition, the efficiency of this system is higher than that of the power generation system [13].

* Corresponding author.
E-mail address: mohammadpour@tabrizu.ac.ir (M. Mohammadpourfard).

https://doi.org/10.1016/j.enconman.2022.115996
Received 26 April 2022; Received in revised form 16 June 2022; Accepted 9 July 2022
Available online 18 July 2022

Nomenclature

Parameters and variables

A	Area (m^2)
c	Cost per exergy unit ($/GJ)
$\dot{C}$	Cost rate ($/yr)
D	Membrane thickness (μm)
D_x	Degassing value (-)
$\dot{E}x$	Exergy rate (kW)
F	Faraday constant (c/mol)
f_k	Exergoeconomic factor (-)
h	Enthalpy (kJ/kg)
I_r	Interest rate (%)
J	Current density (A/m^2)
$\dot{m}$	Mass flow rate (kg/s)
NN	Annual number of hours (h)
n_r	Components expected life (years)
P	Pressure (bar)
$\dot{Q}$	Heat transfer rate (kW)
R	Universal Gas Constant (J/kg.K)
r_k	Relative cost difference (-)
s	Specific entropy (kJ/kg.K)
T	Temperature (K)
V	Voltage (V)
$\dot{W}$	Power (kW)
Z	Equipment purchase cost ($)
$\dot{Z}$	Investment cost rate of components ($/yr)

Acronyms

ARC	Absorption Refrigeration Cycle
CRF	Capital Recovery Factor
COP	Coefficient of Performance
DWH	Domestic Water Heater
ERC	Ejector Refrigeration Cycle
EES	Engineering Equation Solver
EUF	Energy Utilization Factor
GAX	Generator Absorber Heat Exchanger
FBGC	Flash-Binary Geothermal Cycle
GAXA	GAX Absorber
GAXG	GAX Generator
GHG	Greenhouse Gas
GTO	Geothermal Technologies Office
LMTD	Logarithmic Mean Temperature Difference
LNG	Liquefied Natural Gas
ORC	Organic Rankine Cycle
PEME	Proton Exchange Membrane Electrolyzer
PSO	Particle Swarm Optimization
RHX	Refrigerant Heat Exchanger
RO	Reverse Osmosis
SGPP	Sabalan (savalan) Geothermal Power Plant
TEG	Thermoelectric Generator
TUCP	Total Unit Cost of Product

Subscripts

0	Environmental state
a	Anode
abs	Absorber
act	Activation
c	Cathode
CI	Capital Investment
$cond$	Condenser
D	Destruction
eva	Evaporator
EV	Expansion Valve
F	Fuel
FT	Flash tank
gen	Generator
HE	Heat exchanger
in	Inlet
is	Isentropic
L	Loss
net	Net
OM	Operating and maintenance
out	Outlet
P	Product
pu	Pump
ref	Reference
tur	Turbine

Greek symbols

η_{energy}	Energy efficiency
η_{exergy}	Exergy efficiency
λ	Content of water at a distance
φ_r	Maintenance factor (%)
σ	Local ionic conductivity of the membrane

Major researches have been carried out on geothermal energy systems in operating multi-generation cycles, some of which are mentioned here. Nami and Anvari Moghaddam [14] evaluated a cold, heat, and power poly-generation system using geothermal energy. Their system included an Absorption Refrigeration Cycle (ARC), a Domestic Water Heater (DWH), and an Organic Rankine Cycle (ORC). The results showed that the payback period takes about 4.6 years, and the exergy efficiency was 49.6% in the base operating conditions. Ambriz-Díaza et al. [15] presented a tri-generation system based on geothermal energy using ORC, ARC, and dehydrator and analyzed it from advanced exergy and exergoeconomic outlooks. They calculated 8.54 $/h, 7.78 $/h, and 3.52 $/h as the costs of production for electricity, refrigeration, and dehydration, respectively. To achieve an innovative geothermal-driven multi-generation system, Parikhani et al. [16] used the Kalina cycle, Liquefied Natural Gas (LNG), DWH, and an electrolyzer. They calculated the energy and exergy efficiencies 62.74% and 33.82%, respectively. Zare and Takleh [17] proposed two new systems with a geothermal source for simultaneous production of cold, heat, and power. They used energy and exergy analysis to obtain the results and conducted a comparative study. In a similar study, two new systems based on geothermal energy were proposed by Takleh and Zare [18], which were a combination of ORC, Ejector Refrigeration Cycle (ERC), and heater. Their presented system was designed for the summer and winter seasons. In summer, power and refrigeration are produced, and in winter, power and heat are generated. Gnaifaid and Ozcan [19] applied thermodynamic and economic analysis combined with multi-objective optimization for a system based on the Flash-Binary Geothermal Cycle (FBGC), ARC, and Reverse Osmosis (RO) desalination and showed that in the optimal state, exergy efficiency and system cost equal to 58% and 242 $/h, respectively. The system suggested by Ansari et al. [20] was able to produce six products. They used the ORC to generate power and the ARC to generate cold and also assumed the geothermal source temperature to be 573 K. Their results showed that the system exergy efficiency could grow up to 71.6%. Based on the electricity generation in the thermoelectric generator (TEG) [21,22], this unit can be used replacement for the condenser in the geothermal driven systems [23].

Furthermore, hydrogen energy has attracted much attention as a green energy carrier in the recent years. There are various methods to

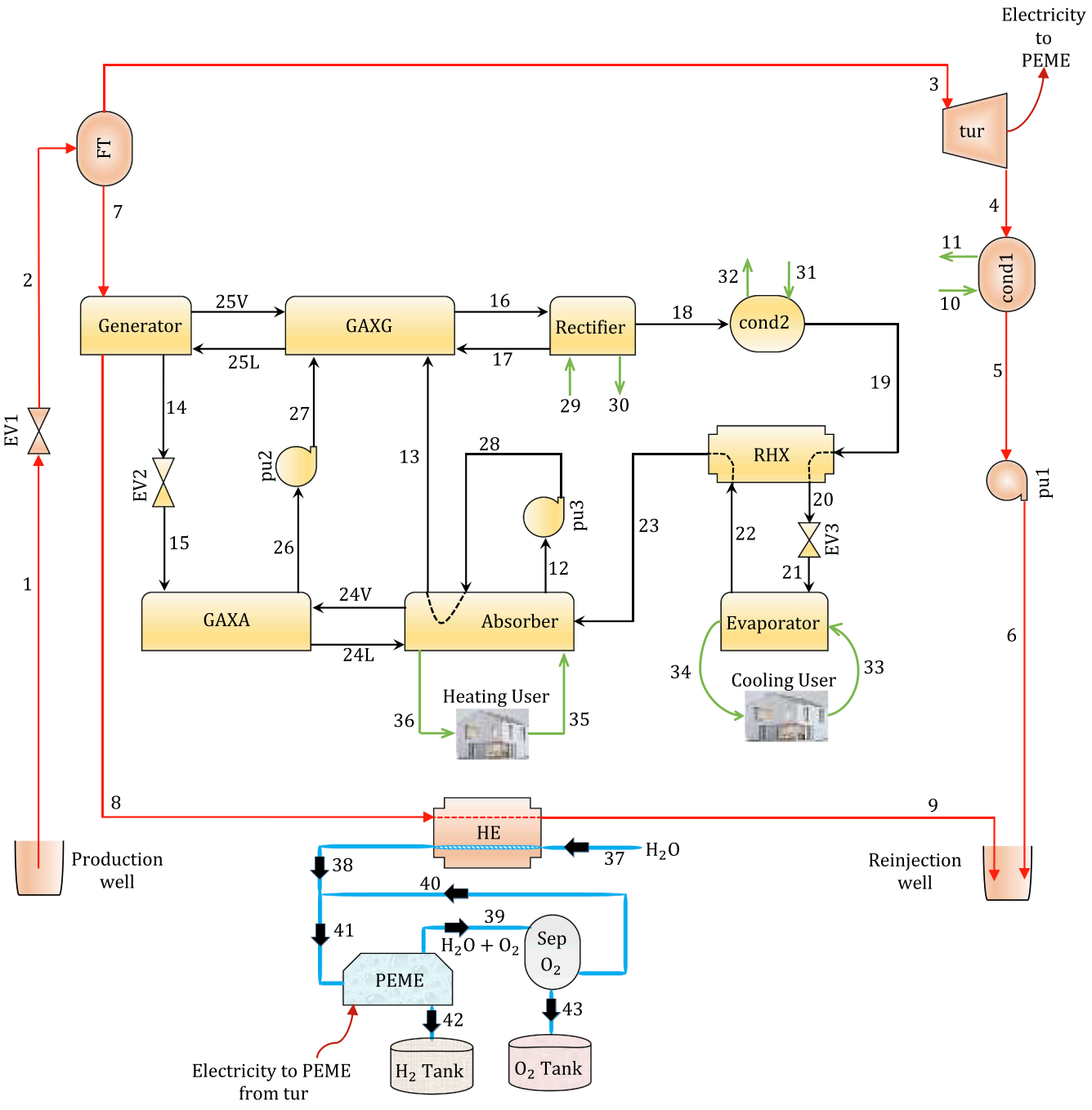

Fig. 1. Schematic of the SGPP-based multi-generation system.

produce hydrogen, but water electrolysis is a promising one especially if renewable energy sources provide its necessary power [24]. Proton Exchange Membrane Electrolyzer (PEME) has many advantages, such as easy design, maintenance and operation [25]. Demir and Dincer investigated a solar-based gas turbine-PEME system [26]. A combined gas turbine-ORC-PEME system for electricity, steam and hydrogen production is studied by Nami and Akrami [27]. They claimed that the costs of their generated steam, hydrogen, and power are 20.6 $/ton, 3.97 $/kg, and 4.81 cent/kWh, respectively. Boyaghchi et al. [28] assessed a biomass-fueled multi-generation with the integration of a PEME and an ORC. Their obtained results showed that an overall thermal efficiency of 77% is achievable. Cao et al. [29] presented a multi-generation system involving a flash binary cycle, a Kalina cycle, an ARC, and a PEME. They used the ARC for the evaporator to refrigerate at -13 °C and also found that as the geothermal water temperature ascends, the exergy efficiency increases.

In practical thermal systems, optimization design problems usually contain two or more conflicting objectives. Hence, Pareto front can offer more reasonable solutions for those opposite objectives. Feili et al. [30] employed the NSGA-II optimization method to optimize their combined cooling, heating, and power system. They selected the Total Unit Cost of Product (TUCP), energy efficiency, and exergy efficiency as the objectives. Their three-objective optimization showed that optimal energy efficiency, exergy efficiency, and TUCP equal 61.61%, 44.46%, and 0.63 $/kWh, respectively. Cao et al. [31] used the NSGA-II optimization method in the Engineering Equation Solver (EES) software for optimizing the multi-generation system powered by geothermal energy, which consists of hydrogen and fresh water production units. They employed R123/R1234ze(e), R123/R1234yf, R600/R1234ze(e), and R600/R1234yf as working fluids and compared the results of

optimization to select the best working fluid. According to their results, R123/R1234ze(e) showed the highest cooling, hydrogen, freshwater production rates, and energy efficiency. Also, the maximum power generation and exergy efficiency belong to R600/R1234ze(e). The particle swarm optimization (PSO) algorithm is a population-based algorithm that is applied to various problems. This optimization method explores the domain of a cost function by setting the particles' trajectories [32]. Zhou et al. [33] proposed a power generation system powered by geothermal energy and did optimization using the PSO algorithm.

In geothermal energy-based multi-generation systems, researchers have used conventional absorption and ejector refrigeration cycles to generate cooling. However, limited attention has been paid to the GAX (Generator-Absorber Heat Exchanger) absorption refrigeration cycle, which branched GAX cycle is one of the cooling cycles based on the GAX In the branched GAX cycle, which is a modified single-effect ARC, a solution of water and ammonia, which is environmentally friendly and has a variable boiling point, can be used as the working fluid. The variability of the boiling point in solutions, which is actually due to the concentration variability in the components, causes the proximity of temperature graphs in heat exchangers and reduces the exergy loss. The branched GAX cycle also has better performance in comparison with the conventional ARCs [34]. Using the branched GAX cycle in the multi-generation system was commenced by Ref. [35], in which the proposed system was able to produce electricity in the ORC, cooling in the branched GAX cycle, and distilled water in the desalination system. Their proposed system was able to generate electricity, cooling, heating, and freshwater. Their results revealed that the highest energy and exergy efficiencies occur using the Isopentane as a working fluid in the ORC, with 79.78% and 33.56%, respectively.

Mohammadi et al. [36] used a gas turbine cycle, ORC equipped with a heat exchanger, branched GAX cycle, and cascade refrigeration cycle to propose a new multi-generation system to generate electricity and cooling. The designed system was started using pure methane fuel. They used thermodynamic, thermoeconomic, and environmental analysis to report their results and then conducted a comparative study between the multi-generation system and the gas turbine power generation system. The results displayed that the multi-generation system has higher energy and exergy efficiencies than the gas turbine power generation system. Also, carbon dioxide emissions of 24,185 tone/yr was reported. In another study, Pourpasha et al. [37] investigated a novel power and refrigeration cogeneration system using the high-temperature ORC with R143a as the working fluid, the low-temperature ORC with water as the working fluid, and the branched GAX cycle. They considered the source temperature to be 703 K and studied the proposed system from thermodynamic and exergoeconomic viewpoints. Their results in basic operating conditions indicated that evaporator with 0.685 MW and pump with 0.0008 MW have the highest and lowest exergy loss among the proposed system components.

The literature survey on geothermal-based multi-generation systems has shown that the available cooling systems are ARC and ERC [38–42]. These cooling systems have a lower coefficient of performance (COP) compared with the branched GAX cycle [34]. Also, the branched GAX cycle has been studied separately and has been used in very limited multi-generation systems. Other points which are seen by surveying literature review are 1) lack of employing PEME next to branched GAX cycle, 2) lack of appealing the branched GAX cycle to produce heating, and 3) lack of applying multi-objective optimization in the branched GAX cycle. Therefore it can be argued that utilizing the branched GAX cycle as a subsystem of geothermal energy is a good idea to reach high cooling capacity. Besides, cooling production is essential due to global warming and production complexity. It is important to note that using fossil fuels to provide the required energy in Iran is a widespread technology, which leads to the production of greenhouse gases. It is worth noting that eighteen locations with geothermal energy possibilities have been determined in Iran. One of them is Sabalan (Savalan) geothermal power plant (SGPP), which is located in Meshkinshahr city [43].

In light of the above discussion, a new multi-generation configuration working with a single flash cycle, a branched GAX cycle, and an electrolyzer, powered by SGPP, is proposed in this paper. The proposed system is capable of producing generate electricity, cooling, heating, and hydrogen simultaneously. The branched GAX cycle is used in the saturated liquid part of the flash tank outlet, which has high thermodynamic properties and mass flow rate, leading to increased cooling and heating outputs. The electricity is generated in a single flash cycle, and part of it is used to drive the electrolyzer to produce hydrogen. For scrutinizing the performance of the proposed system, thermodynamic and exergoeconomic outlooks are used, and then two-objective optimization, by using the TUCP and energy efficiency as objectives, is utilized to find the optimum operating conditions. Considering the emphasis on determining the novelties and innovations in an academic study, the most distinguished points of this paper are summarized below:

- Evaluation of a novel multi-generation system benefiting from Sabalan (Savalan) geothermal power plant source in a novel application that has not been studied yet.
- Simultaneous generation of three forms of energy (i.e., electricity, heating, and cooling), as well as one different energy-based product (i.e., hydrogen) via a modified and efficient multi-generation system.
- Incorporating of a branched GAX cycle in the saturated liquid part of the flash tank outlet to produce the cooling and heating.
- Applying thermodynamic and exergoeconomic outlooks to evaluate the system performance.
- Conducting a two-objective optimization for reaching optimum working conditions.
- Making a comparison with similar works that are powered by Sabalan (Savalan) geothermal power plant.

2. System description

Fig. 1 illustrates the supposed multi-generation system powered by SGPP. The presented system includes a single flash cycle, a branched GAX cycle, and an electrolyzer, which is able to produce electricity, cooling, heating, and hydrogen. As can be seen, liquid water is extracted from the production well (state 1) and is passed through EV1. Then it goes to the flash tank as a two-phase flow (state 2). After passing through the flash tank, the saturated vapour (state 3) is directed to the turbine to produce electricity and is then condensed at 30 °C (state 4 to state 5). On the other hand, the saturated liquid (state 7) is used as a heat source to run the branched GAX cycle through the generator (state 7 to state 8) and electrolyzer via the heat exchanger (state 8 to state 9). Condensing water is pumped by pump 1 to reinjection pressure (state 5 to state 6), and states 6 and 9 are finally reinjected into the injection well.

According to Fig. 1, the branched GAX cycle consists of the generator, evaporator, condenser, rectifier, a Refrigerant Heat Exchanger (RHX), GAX Generator (GAXG), GAX Absorber (GAXA), two pumps, and two expansion valves. The saturated rich solution is ejected from the absorber and is pumped to the low-temperature side of the generator. In the generator, the solution absorbs heat from state 7. This solution is boiled in the generator and produces vapour with a high ammonia concentration. Vapour and liquid are delivered to the low-temperature side and high-temperature side of the generator, respectively. The weak solution is ejected from the generator and is passed through EV2, GAXA, and pump 2, and is finally entered into the GAXG. Having left the generator, the vapour ammonia passes through the rectifier and goes towards condenser 2 to undergo the condensing process. It is important to note that the saturated liquid goes back to the generator from the rectifier. Then, condensing ammonia passes through RHX and EV3, respectively, and goes to the evaporator to produce cooling. The liquid refrigerant absorbs heat in the RHX and vaporizes. Finally, it goes into the absorber to complete the cycle. Ultimately, the electrolyzer is

Table 1
Details of mass, energy, and exergy relations for the proposed system components.

Component	Mass equation	Energy equation	Exergy destruction
Condenser 1	$\dot{m}_{11}=\dot{m}_{10},\ \dot{m}_4=\dot{m}_5$	$\dot{Q}_{cond1}=\dot{m}_4(h_4-h_5)$,$\dot{Q}_{cond1}=\dot{m}_{11}(h_{11}-h_{10})$	$\dot{E}x_D^{cond1}=(\dot{E}x_4-\dot{E}x_5)-(\dot{E}x_{11}-\dot{E}x_{10})$
Turbine	$\dot{m}_3=\dot{m}_4$	$\dot{W}_{tur}=\dot{m}_4(h_3-h_4)$, $\eta_{is.tur}=(h_3-h_4)/(h_3-h_{4s})$	$\dot{E}x_D^{tur}=\left(\dot{E}x_3-\dot{E}x_4\right)-\dot{W}_{tur}$
FT	$\dot{m}_2=\dot{m}_7+\dot{m}_3$	$\dot{m}_2h_2=\dot{m}_7h_7+\dot{m}_3h_3$	$\dot{E}x_D^{FT}=\dot{E}x_2-(\dot{E}x_7+\dot{E}x_3)$
EV1	$\dot{m}_1=\dot{m}_2$	$h_1=h_2$	$\dot{E}x_D^{EV1}=\dot{E}x_1-\dot{E}x_2$
Pump1	$\dot{m}_5=\dot{m}_6$	$\dot{W}_{pu1}=\dot{m}_5(h_6-h_5)$, $\eta_{is.pu1}=(h_{6s}-h_5)/(h_6-h_5)$	$\dot{E}x_D^{pu1}=\dot{W}_{pu1}-\left(\dot{E}x_6-\dot{E}x_5\right)$
HE	$\dot{m}_8=\dot{m}_9,\ \dot{m}_{37}=\dot{m}_{38}$	$\dot{Q}_{HE}=\dot{m}_8(h_8-h_9)$ $\dot{Q}_{HE}=\dot{m}_{38}(h_{38}-h_{37})$	$\dot{E}x_D^{HE}=(\dot{E}x_8-\dot{E}x_9)-(\dot{E}x_{38}-\dot{E}x_{37})$
Absorber	$\dot{m}_{15}+\dot{m}_{23}=\dot{m}_{12}+\dot{m}_{26}$, $\dot{m}_{15}x_{15}+\dot{m}_{23}x_{23}=\dot{m}_{12}x_{12}+\dot{m}_{26}x_{26}$	$\dot{Q}_{abs.total}=\dot{m}_{15}h_{15}+\dot{m}_{23}h_{23}+\dot{m}_{28}h_{28}-\dot{m}_{26}h_{26}-\dot{m}_{12}h_{12}-\dot{m}_{13}h_{13}$, $\dot{Q}_{abs}=\dot{Q}_{abs.total}-\dot{Q}_{available}$, $\dot{Q}_{abs}=\dot{m}_{36}(h_{36}-h_{35})$	$\dot{E}x_D^{gen\&abs}=(\dot{E}x_7-\dot{E}x_8)-(\dot{E}x_{14}+\ +\dot{E}x_{16}+\dot{E}x_{12}+\dot{E}x_{26}+\dot{E}x_{36}-\dot{E}x_{27}-\dot{E}x_{17}-\dot{E}x_{15}-\dot{E}x_{28}-\dot{E}x_{23}-\dot{E}x_{35}$
GAXA	$\dot{m}_{26}+\dot{m}_{24L}=\dot{m}_{15}+\dot{m}_{24V}$, $\dot{m}_{26}x_{26}+\dot{m}_{24L}x_{24L}=\dot{m}_{15}x_{15}+\dot{m}_{24V}x_{24V}$	$\dot{Q}_{available}=\dot{m}_{15}h_{15}+\dot{m}_{24v}h_{24v}-\dot{m}_{26}h_{26}-\dot{m}_{24L}h_{24L}$,	
Generator	–	$\dot{Q}_{gen.total}=\dot{m}_{16}h_{16}+\dot{m}_{14}h_{14}-\dot{m}_{13}h_{13}-\dot{m}_{27}h_{27}-\dot{m}_{17}h_{17}$, $\dot{Q}_{gen}=\dot{Q}_{gen.total}-\dot{Q}_{required}$, $\dot{Q}_{gen}=\dot{m}_7(h_7-h_8)$	
GAXG	$\dot{m}_{27}+\dot{m}_{25V}+\dot{m}_{13}+\dot{m}_{17}=\dot{m}_{16}+\dot{m}_{25L}$, $\dot{m}_{27}x_{27}+\dot{m}_{25V}x_{25V}+\dot{m}_{13}x_{13}+\dot{m}_{17}x_{17}=\dot{m}_{16}x_{16}+\dot{m}_{25L}x_{25L}$	$\dot{Q}_{required}=\dot{m}_{16}h_{16}+\dot{m}_{25L}h_{25L}-\dot{m}_{27}h_{27}-\dot{m}_{25V}h_{25V}-\dot{m}_{13}h_{13}-\dot{m}_{17}h_{17}$,	
RHX	$\dot{m}_{19}=\dot{m}_{20},\ \dot{m}_{22}=\dot{m}_{23}$	$\dot{Q}_{RHX}=\dot{m}_{19}(h_{19}-h_{20})$, $\dot{Q}_{RHX}=\dot{m}_{22}(h_{23}-h_{22})$, $\epsilon_{RHX}=\frac{T_{19}-T_{20}}{T_{19}-T_{22}}$	$\dot{E}x_D^{RHX}=(\dot{E}x_{19}-\dot{E}x_{20})-(\dot{E}x_{23}-\dot{E}x_{22})$
Condenser 2	$\dot{m}_{18}=\dot{m}_{19},\ \dot{m}_{32}=\dot{m}_{31}$	$\dot{Q}_{cond2}=\dot{m}_{18}(h_{18}-h_{19})$,$\dot{Q}_{cond2}=\dot{m}_{32}(h_{32}-h_{31})$	$\dot{E}x_D^{cond2}=(\dot{E}x_{18}-\dot{E}x_{19})-(\dot{E}x_{32}-\dot{E}x_{31})$
Evaporator	$\dot{m}_{22}=\dot{m}_{21},\ \dot{m}_{34}=\dot{m}_{33}$	$\dot{Q}_{eva}=\dot{m}_{22}(h_{22}-h_{21})$,$\dot{Q}_{eva}=\dot{m}_{33}(h_{33}-h_{34})$	$\dot{E}x_D^{eva}=(\dot{E}x_{21}-\dot{E}x_{22})-(\dot{E}x_{34}-\dot{E}x_{33})$
Rectifier	$\dot{m}_{17}+\dot{m}_{18}=\dot{m}_{16}$, $\dot{m}_{17}x_{17}+\dot{m}_{18}x_{18}=\dot{m}_{16}x_{16}$	$\dot{Q}_{rect}=\dot{m}_{30}(h_{30}-h_{29})$,$\dot{Q}_{rect}=\dot{m}_{16}h_{16}-\dot{m}_{17}h_{17}-\dot{m}_{18}h_{18}$	$\dot{E}x_D^{rect}=(\dot{E}x_{16}-\dot{E}x_{17}-\dot{E}x_{18})-(\dot{E}x_{30}-\dot{E}x_{29})$
Pump2	$\dot{m}_{26}=\dot{m}_{27}$	$\dot{W}_{pu2}=\dot{m}_{27}(h_{27}-h_{26})$, $\eta_{is.pu2\&3}=(h_{27s}-h_{26})/(h_{27}-h_{26})$	$\dot{E}x_D^{pu2}=\dot{W}_{pu2}-\left(\dot{E}x_{27}-\dot{E}x_{26}\right)$
Pump3	$\dot{m}_{28}=\dot{m}_{12}$	$\dot{W}_{pu3}=\dot{m}_{28}(h_{28}-h_{12})$, $\eta_{is.pu2\&3}=(h_{28s}-h_{12})/(h_{28}-h_{12})$	$\dot{E}x_D^{pu3}=\dot{W}_{pu3}-\left(\dot{E}x_{28}-\dot{E}x_{12}\right)$
EV2	$\dot{m}_{14}=\dot{m}_{15}$	$h_{14}=h_{15}$	$\dot{E}x_D^{EV2}=\dot{E}x_{14}-\dot{E}x_{15}$
EV3	$\dot{m}_{20}=\dot{m}_{21}$	$h_{20}=h_{21}$	$\dot{E}x_D^{EV3}=\dot{E}x_{20}-\dot{E}x_{21}$
Separation O_2	$\dot{m}_{43}+\dot{m}_{40}=\dot{m}_{39}$	$\dot{m}_{43}h_{43}+\dot{m}_{40}h_{40}=\dot{m}_{39}h_{39}$	$\dot{E}x_D^{sep,O_2}=\dot{E}x_{39}-(\dot{E}x_{43}+\dot{E}x_{40})$
PEME	$\dot{m}_{43}+\dot{m}_{40}=\dot{m}_{39}$	See PEME section	$\dot{E}x_D^{PEME}=\dot{W}_{PEME}+\dot{E}x_{39}-\left(\dot{E}x_{43}+\dot{E}x_{40}\right)$

operated using one-tenth of the electricity generated by the turbine and water to produce O_2 (state 43) and H_2 (state 42). The operation of the mentioned subsystem has been thoroughly examined in previous papers [44–46].

EES software is used to find the properties of working fluids at each state [47], and modelling of the proposed system is done beneath assumptions [48–50]

- All components and their passing streams are in a steady-state.
- Pressure drops in all components are neglected.
- Pure water is exploited from the geothermal production well.
- Working fluids have saturated conditions at the flash tank, evaporator, absorber, and condensers outlet.
- Expansion valves operate at the enthalpy constant conditions.
- Isentropic efficiency is used in the turbine and pumps modeling. (see Table 5)
- Degassing value is assumed 0.30 and is defined as $D_x=(x_{12}-x_{14})$.

A few points to keep in mind, the first point is cooling water temperature, which is below 30 °C. Forasmuch as the SGPP is located in Meshkinshahr city, which is one of the cold cities in Iran. Being near the high Sabalan (Savalan) Mountains, it enjoys a moderate mountainous climate. So, the temperature below 30 °C throughout the year for cooling water is available. The second point is selecting operational conditions for the proposed system components. It is worth noting that production well properties (state 1) are chosen based on the real data (see Table 5). Moreover, other properties are selected based on the previous literature and system operation. For instance, the pressure of the flash tank is chosen as 5.2-7 bar to satisfy the required temperature of state 14. The temperature outlet in the branched GAX cycle (state 14) is about 415 K. It should be noted that the temperature of state 7 must be more than the temperature of state 14. Mass flows are calculated based on the mass flow of the SGPP.

3. Mathematical modeling

With regards to the importance of PEME, this unit is introduced with details as follows:

3.1. PEME modeling

One-tenth of electricity generation in the turbine is devoted to the electrolyzer. So, related reactions for the cathode and anode sides and overall form are defined as below [51]:

Table 2
Equipment purchase cost for the system components.

Component	Cost equations ($)	$CEPCI_{Ref}$	Ref.
Heat exchangers	$Z_{HEs} = 30800 + 750 \times (A_{HEs})^{0.81}$	$CEPCI_{1985} = 325$	[54]
Turbine	$Z_{tur} = 6000 \times (\dot{W}_{tur})^{0.7}$	$CEPCI_{2010} = 550.8$	[55]
Flash tank	$Z_{FT} = 4.34 \times C_{FT}\log C_{FT}=3.4974+0.4485\times\log V_{FT}+0.1074\ \log^2 V_{FT}$ $V_{FT} = \frac{\pi}{4}D^2(L_A + L_B)$, $L_A = 7D_{ip}$, $L_b = 4.5D_{ip}, D = 3D_{ip}$ $D_{ip}=(\frac{4\times A_{ip}}{\pi})^{0.5}$, $A_{ip} = \frac{\dot{V}}{V_t}$, $V_t = 0.069\times(\frac{\rho_l - \rho_V}{\rho_l})^{0.5}$	$CEPCI_{2016} = 541.7$	[56]
Pump 1	$Z_{pu1} = 1120 \times (\dot{W}_{pu1})^{0.80}$	$CEPCI_{2010} = 550.8$	[57]
Pumps 2,3	$Z_{pu2,3} = 3450 \times (\dot{W}_{pu2,3})^{0.7}$	$CEPCI_{2010} = 550.8$	[58]
PEME	$Z_{PEME} = 1000 \times \dot{W}_{PEME}$	$CEPCI_{2010} = 550.8$	[59]
EVs	$Z_{EV} = 114.5 \times \dot{m}$	$CEPCI_{2000} = 394.1$	[60]

Table 3
Auxiliary equations and exergy cost rate balances for the presented system components.

Component	Cost rate balance	Auxiliary equation
Condenser 1	$\dot{C}_5 + \dot{C}_{11}=\dot{C}_4 + \dot{C}_{10} + \dot{Z}_{cond1}$	$c_4=c_5, c_{10}=0$
Turbine	$\dot{C}_4 + \dot{C}_{W,tur}=\dot{C}_3 + \dot{Z}_{tur}$	$c_3=c_4$
FT	$\dot{C}_7 + \dot{C}_3 = \dot{C}_2 + \dot{Z}_{FT}$	$c_7=c_3$
EV1	$\dot{C}_2=\dot{C}_1 + \dot{Z}_{EV1}$	-
Pump 1	$\dot{C}_6=\dot{C}_5 + \dot{Z}_{pu1} + \dot{C}_{W,pu1}$	$c_{W,pu1}=c_{w,tur}$
HE	$\dot{C}_9 + \dot{C}_{38}=\dot{C}_8 + \dot{C}_{37} + \dot{Z}_{HE}$	$c_9=c_8, c_{37}=0$
Absorber	$\dot{C}_{12} + \dot{C}_{13} + \dot{C}_{26} + \dot{C}_{36}=\dot{C}_{23} + \dot{C}_{28} + \dot{C}_{15} + \dot{C}_{35} + \dot{Z}_{abs}$	$c_{35}=0$, $(\dot{C}_{23} + \dot{C}_{15})/(\dot{E}x_{23} + \dot{E}x_{15})=\dot{C}_{12}/\dot{E}x_{12}$ $(\dot{C}_{28} + \dot{C}_{15})/(\dot{E}x_{28} + \dot{E}x_{15})=\dot{C}_{13}/\dot{E}x_{13}$ $\dot{C}_{13}/\dot{E}x_{13}=\dot{C}_{26}/\dot{E}x_{26}$
GAXA	$\dot{C}_{26} + \dot{C}_{24L} = \dot{C}_{24V} + \dot{C}_{15} + \dot{Z}_{GAXA}$	$(\dot{C}_{24L} -(\dot{C}_{24V} + \dot{C}_{15}))/(\dot{E}x_{24L} -(\dot{E}x_{24V} + \dot{E}x_{15}))= (\dot{C}_{26} -(\dot{C}_{24V} + \dot{C}_{15}))/(\dot{E}x_{26} -(\dot{E}x_{24V} + \dot{E}x_{15}))$
Generator	$\dot{C}_8 + \dot{C}_{14} + \dot{C}_{16}=\dot{C}_7 + \dot{C}_{27} + \dot{C}_{13} + \dot{C}_{17} + \dot{Z}_{gen}$	$c_7=c_8$, $(\dot{C}_{16} -\dot{C}_{13})/(\dot{E}x_{16} -\dot{E}x_{13})= (\dot{C}_{14} -\dot{C}_{13})/(\dot{E}x_{14} -\dot{E}x_{13})$
GAXG	$\dot{C}_{16} + \dot{C}_{25L} = \dot{C}_{25V} + \dot{C}_{13} + \dot{C}_{27} + \dot{C}_{17} + \dot{Z}_{GAXG}$	$(\dot{C}_{25L} -(\dot{C}_{25V} + \dot{C}_{13} + \dot{C}_{27} + \dot{C}_{17}))/(\dot{E}x_{25L} -(\dot{E}x_{25V} + \dot{E}x_{13} + \dot{E}x_{27} + \dot{E}x_{17}))= (\dot{C}_{16} -(\dot{C}_{25V} + \dot{C}_{13} + \dot{C}_{27} + \dot{C}_{17}))/(\dot{E}x_{16} -(\dot{E}x_{25V} + \dot{E}x_{13} + \dot{E}x_{27} + \dot{E}x_{17}))=$
RHX	$\dot{C}_{20} + \dot{C}_{23}=\dot{C}_{19} + \dot{C}_{22} + \dot{Z}_{RHX}$	$c_{19}=c_{20}$
Condenser 2	$\dot{C}_{19} + \dot{C}_{32}=\dot{C}_{18} + \dot{C}_{31} + \dot{Z}_{cond2}$	$c_{18}=c_{19}, c_{31}=0$
Evaporator	$\dot{C}_{22} + \dot{C}_{34}=\dot{C}_{21} + \dot{C}_{33} + \dot{Z}_{eva}$	$c_{21}=c_{22}, c_{33}=0$
Rectifier	$\dot{C}_{30} + \dot{C}_{18} + \dot{C}_{17}=\dot{C}_{16} + \dot{C}_{29} + \dot{Z}_{rect}$	$c_{18}=c_{19}, c_{29}=0$ $(\dot{C}_{18} -\dot{C}_{16})/(\dot{E}x_{18} -\dot{E}x_{16})= (\dot{C}_{17} -\dot{C}_{16})/(\dot{E}x_{17} -\dot{E}x_{16})$
Pump 2	$\dot{C}_{27}=\dot{C}_{26} + \dot{Z}_{pu2} + \dot{C}_{W,pu2}$	$c_{W,pu2}=c_{w,tur}$
Pump 3	$\dot{C}_{28}=\dot{C}_{12} + \dot{Z}_{pu3} + \dot{C}_{W,pu3}$	$c_{W,pu3}=c_{w,tur}$
EV2	$\dot{C}_{15}=\dot{C}_{14} + \dot{Z}_{EV2}$	–
EV3	$\dot{C}_{21}=\dot{C}_{20} + \dot{Z}_{EV2}$	–
Separation O_2	$\dot{C}_{43} + \dot{C}_{40}=\dot{C}_{39} + \dot{Z}_{sep,O_2}$	$c_{43}=c_{40}$
PEME	$\dot{C}_{42} + \dot{C}_{39}=\dot{C}_{41} + \dot{Z}_{PEME}+\dot{C}_{W,PEME}$	$c_{W,PEME}=c_{w,tur}$, $c_{42}=c_{39}$

$$H_2O \rightarrow 2H^+ + 0.5O_2 + 2e^- (\text{Anode side reaction}) \quad (1)$$

$$2H^+ + 2e^- \rightarrow H_2 (\text{Cathode side reaction}) \quad (2)$$

$$H_2O + \text{energy} \rightarrow H_2 + 0.5O_2 (\text{Overall reaction}) \quad (3)$$

The hydrogen production rate can be calculated as follows [50]:

$$\dot{N}_{H_2} = \frac{J}{2F} \quad (4)$$

Here, F and J are expressed as Faraday constant and current density, respectively.

The required electricity to drive the electrolyzer is equal to [50]:

$$\dot{W}_{PEME} = \frac{\dot{W}_{tur}}{10} = J \times V \quad (5)$$

Here, V is the voltage of the electrolyzer and can be calculated by [50]:

$$V = V_0 + V_{act,a} + V_{act,c} + V_{ohm} \quad (6)$$

where V_0, $V_{act,a}$, $V_{act,c}$, and V_{ohm} are the reversible potential, anode-side activation potential, activation potential of cathode-side, and ohmic potential, respectively.

The reversibility potential can be calculated as follows [50]:

$$V_0 = 1.229 - 8.5 \times 10^{-4}(T_{PEME} - 298) \quad (7)$$

Anode-side and cathode-side activation potential can be calculated by [50]:

$$V_{act,i} = \frac{R \times T_{PEME}}{F}\sinh^{-1}\left(\frac{J}{2 \times J_{0,i}}\right),\ i = a, c \quad (8)$$

where $J_{0,i}$ is the current density of electrolyzer exchange and is obtained from [50]:

$$J_{0,i} = J_i^{ref} \times \exp\left(-\frac{E_{act,i}}{R \times T_{PEME}}\right),\ i = a, c \quad (9)$$

And the ohmic potential is expressed as [50]:

$$V_{ohm} = J \times R_{PEME} \quad (10)$$

Here, R_{PEME} is ohmic resistance and is defined as [50]:

$$R_{PEME} = \int_0^L \frac{dx}{\sigma_{PEME}[\lambda(x)]} \quad (11)$$

Here, $[\lambda(x)]$ and $\sigma_{PEME}[\lambda(x)]$ indicate the amount of water at distance x and the local unique coefficient of conductivity, respectively, and can be calculated from the following equations [50]:

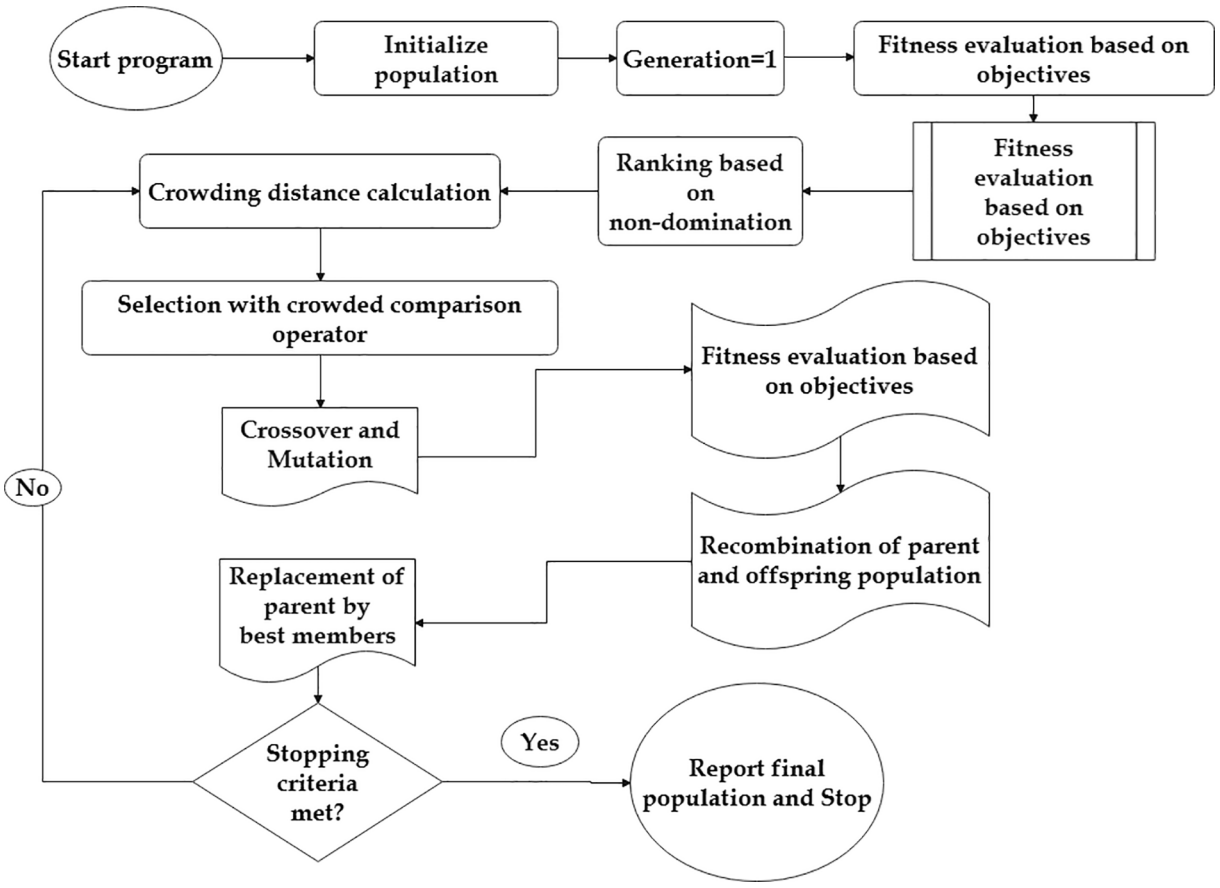

Fig. 2. The flowchart of the NSGA-II optimization method.

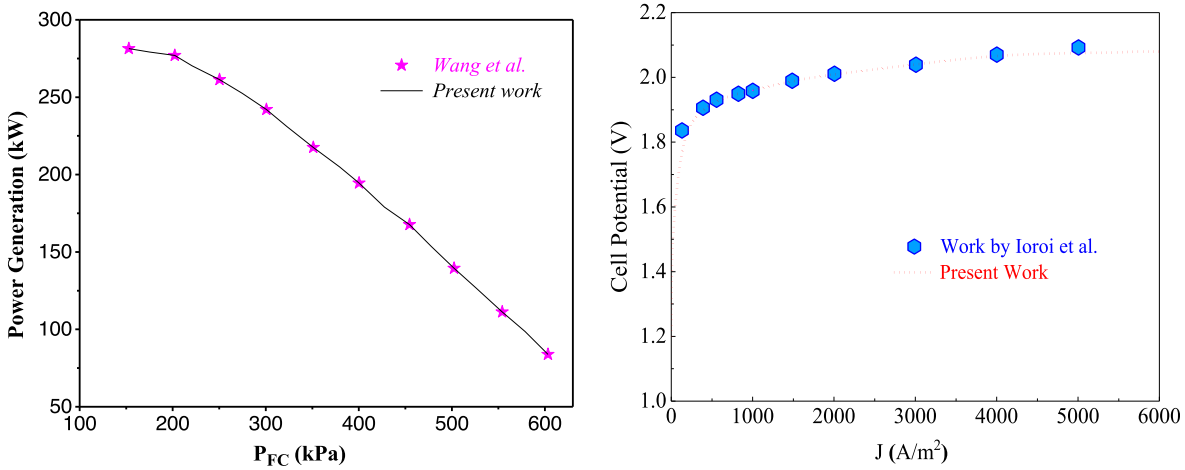

Fig. 3. Validation outcomes for (a) single flash geothermal cycle [68] and (b) Electrolyser unit [69].

$$\lambda(x) = \frac{\lambda_a - \lambda_c}{D} x + \lambda_c \tag{12}$$

$$\sigma_{PEME}[\lambda(x)] = [0.5139\lambda(x) - 0.326]\left[1268\left(\frac{1}{303} - \frac{1}{T_{PEME}}\right)\right] \tag{13}$$

3.2. Thermodynamic investigation

Balancing equations of mass and energy are defined based on the relations beneath.

$$\sum \dot{m}_{in} = \sum \dot{m}_{out} \tag{14}$$

$$\dot{Q} - \dot{W} = \sum \dot{m}_{out}(h_{out}) - \sum \dot{m}_{in}(h_{in}) \tag{15}$$

Exergy analysis is a crucial and qualitative strategy to investigate thermodynamic systems. The exergy equation is expressed as:

$$\dot{E}_Q + \sum \dot{m}_{in} e_{in} = \dot{E}_W + \sum \dot{m}_{out} e_{out} + \dot{E}_D \tag{16}$$

With regards to the above relations and Fig. 1, Table 1 shows the

Table 4
Comparison of COP with Refs. [70–72].

Parameter	Reference	Current study	Relative error (%)	Operating conditions
Yari et al. [70]				T_{eva}(K) = 278.15T_{gen}(K) = 436.45T_{cond}(K) = 313.15D_x = 5
COP	1.103	1.098	0.45	
Udayakumar [71]				
COP	1.08	1.098	1.66	
Herold et al. [72]				
COP	1.10	1.098	0.18	

Table 5
Input data.

Parameter	Value	Ref.
Sabalan (Savalan) geothermal power plant		
Pressure of geothermal water,P_1 (bar)	12	[48]
Enthalpy of geothermal water,h_1 (kJ/kg)	1000	[48]
Mass flow rate of geothermal water,$\dot{m}_1$ (kg/s)	45	[48]
Flash tank pressure, P_{FT}(bar)	5.2-7	assumed
Turbine expansion ratio, ER_{tur}	120	[48]
Turbine isentropic efficiency, $\eta_{is,tur}$ (%)	85	[48]
Pump1 isentropic efficiency, $\eta_{is,pu1}$ (%)	85	[48]
Branched GAX cycle		
Generator temperature, T_{gen}(K)	400-420	assumed
Condenser 2 temperature, T_{cond2}(K)	308-328	assumed
Evaporator temperature, T_{eva}(K)	270-280	assumed
Degassing value, D_x	0.2-0.37	assumed
The effectiveness of heat exchanger, $\in_{RHX}$	0.8	[58,73]
Pumps 2&3 isentropic efficiency, $\eta_{is,pu2,3}$ (%)	50	[58,73]
Condenser, absorber, rectifier, and evaporator inlets water temperature, T_{in}(K)	298	[58,73]
The vapor quality of the two-phase solution leaving the evaporator, $Qu_{out,eva}$	0.94	[58,73]
Ammonia mass fraction of the rectifier outlet, $X_{out,rect}$	0.995	[58,73]
PEM electrolyzer unit		
PEME temperature,T_{PEME} (K)	353	[45]
Anode pre-expotential factor,J_a^{ref} (A.m^{-2})	1.7×10^5	[45]
Anode activation energy, $E_{act,a}$ (kJ.mol^{-1})	76	[45]
Faraday constant, F (C.mol^{-1})	96,486	[45]
Membrane thickness, D (μm)	100	[45]
Cathode pre-expotential factor, J_a^{ref} (A.m^{-2})	4.6×10^3	[45]
Cathode activation energy, $E_{act,c}$ (kJ.mol^{-1})	18	[45]
$_c$ (1.Ω^{-1})λMembrane cathode surface water,	10	[45]
$_a$ (1.Ω^{-1})λMembrane anode surface water,	14	[45]
Economic parameters for cost evaluation		
Annual operational hours, NN (hour)	7000	[74]
Unit cost of geofluid exergy,C_1($/GJ)	1.3	[74]
Maintenance factor,φ_r	1.06	[74]
Annual interest rate, I_r (%)	15	[74]
Lifetime of the systems,n_r(years)	20	[74]
NSGA-II algorithm		
Probability of mutation	0.01	-
Probability of crossover	0.8	-
Maximum number of generation	150	-
Population size	200	-

equations of the mass, energy, and exergy for each component of the proposed system.

The first law of thermodynamics provides a suitable benchmark for the evaluation of system performance, which is Energy efficiency. Therefore, for the proposed system, with the ability to generate electricity, heating, cooling, and hydrogen, energy efficiency can be expressed as below:

$$\eta_{energy} = \frac{\dot{W}_{net} + \dot{Q}_{cooling} + \dot{Q}_{heating} + \dot{m}_{42} LHV_{H_2}}{\dot{m}_1 h_1 - \dot{m}_6 h_6 - \dot{m}_9 h_9} \tag{17}$$

here, $\dot{W}_{net}$, $\dot{Q}_{cooling}$, and $\dot{Q}_{heating}$ denote pure electricity, cooling load, and heating load, and are defined as below:

$$\dot{W}_{net} = \dot{W}_{tur} - \dot{W}_{pu1} - \dot{W}_{pu2} - \dot{W}_{pu3} - \dot{W}_{PEME} \tag{18}$$

$$\dot{Q}_{abs} = \dot{Q}_{heating} = \dot{m}_{36}(h_{36} - h_{35}) \tag{19}$$

$$\dot{Q}_{eva} = \dot{Q}_{cooling} = \dot{m}_{36}(h_{33} - h_{34}) \tag{20}$$

Also, for the branched GAX cycle, the Energy Utilization Factor (EUF_{GAX}) can be defined as below:

$$EUF_{GAX} = \frac{\dot{Q}_{cooling} + \dot{Q}_{heating}}{\dot{Q}_{gen} + \dot{W}_{pu2} + \dot{W}_{pu3}} \tag{21}$$

Likewise, exergy efficiency can be expressed as:

$$\eta_{exergy} = \frac{\dot{W}_{net} + \dot{E}x_{34} + \dot{E}x_{36} + \dot{E}x_{42}}{\dot{E}x_1 - \dot{E}x_6 - \dot{E}x_9} \tag{22}$$

3.3. Exergoeconomic investigation

The cost balance relation for the system components is presented as below [52]:

$$\dot{C}_{q,k} = \sum \dot{C}_{in,k} + \dot{Z}_k = \dot{C}_{w,k} + \sum \dot{C}_{out,k} \tag{23}$$

here $\dot{C}_{q,k}$ and $\dot{C}_{w,k}$ denote cost rate of heat exchange and output electricity, and $\dot{C}_{in,k}$ and $\dot{C}_{out,k}$ indicate the cost rate of inlet and outlet flows for the kth component

Cost rate, unit cost, and exergy are related together via beneath equation [52]:

$$\dot{C}_k = c_k \dot{E}x_k \tag{24}$$

For the kth component, the relative cost difference is defined as below:

$$r_k = \left(c_{P,k} - c_{F,k}\right)/c_{F,k} \tag{25}$$

For the kth component, the exergoeconomic factor is:

$$f_k = \dot{Z}_k / \left(\dot{Z}_k + \dot{Z}_{D,k}\right) \tag{26}$$

in which the cost rate of the total input stream is [52]:

$$\dot{Z}_k = \dot{Z}_k^{CI} + \dot{Z}_k^{OM} = CRF \times \frac{\varphi_r \times 365 \times 24}{NN} \times Z_k \tag{27}$$

where Z_k is the total cost for the kth component, $\dot{Z}_k^{OM}$ and $\dot{Z}_k^{CI}$ are the cost rate of the operating and maintenance and investment for the kth component, φ_r is the maintenance factor, NN is the annual operating hours, and CRF is the capital recovery factor defined as [52]:

$$CRF = \frac{I_r(1+I_r)^{n_r}}{(1+I_r)^{n_r} - 1} \tag{28}$$

In the relation above, I_r and n_r are interest rate and system life.

Additionally, to translate the calculated values regarding 2021 for the kth component into real values, CEPCI, which is defined below, is applied [53]:

$$\dot{Z}_{k,2021} = \dot{Z}_k \left(\frac{CEPCI_{2021}}{CEPCI_{ref,year}}\right) \tag{29}$$

Table 6
Thermodynamic properties and exergoeconomic outcomes for each state of the proposed system at the base case.

State	T(K)	P(bar)	h(kg/kJ)	s(kg/kJ K)	$\dot{m}$(kg/s)	x	$\dot{E}x$(kW)	$\dot{C}$($/h)	c($/kWh)
1	461.1	12	1000	2.653	45	-	9720	45.49	0.00468
2	425	5.2	1000	2.707	45	-	8996	45.69	0.005079
3	425	5.2	2749	6.821	7.676	-	5541	28.14	0.005079
4	302.8	0.04167	2163	7.163	7.676	-	261.1	1.326	0.005079
5	302.8	0.04167	124.3	0.432	7.676	-	19.59	0.0995	0.005079
6	302.8	5.2	124.8	0.4319	7.676	-	23.41	0.2532	0.01082
7	425	5.2	640.4	1.861	37.32	-	3455	22.46	0.006502
8	415.2	5.2	597.9	1.76	37.32	-	2995	19.47	0.006502
9	415.1	5.2	597.8	1.76	37.32	-	2994	19.47	0.006502
10	298.2	1.012	104.8	0.3669	748	-	1869	0	0
11	303.2	1.012	125.8	0.4365	748	-	1998	27.8	0.01391
12	309.8	4.784	-75.28	0.3887	3.598	0.5111	36485	565.5	0.0155
13	353	15.48	123.5	0.9849	3.598	0.5111	36560	566.1	0.01548
14	418.2	15.48	489.4	1.823	2.795	0.2111	12154	186.6	0.01536
15	381.4	4.784	489.4	1.851	2.795	0.2111	12130	186.7	0.01539
16	353	15.48	1426	4.57	1.453	0.9877	28790	445.3	0.01547
17	353	15.48	123.5	0.9849	0.0218	0.5111	221.5	5.946	0.02684
18	340.4	15.48	1383	4.445	1.431	0.995	28555	441.7	0.01547
19	313.2	15.48	187.3	0.6622	1.431	0.995	28458	440.2	0.01547
20	285.3	15.48	53.41	0.2146	1.431	0.995	28457	440.2	0.01547
21	276.2	4.784	53.41	0.2225	1.431	0.995	28454	440.2	0.01547
22	278.2	4.784	1198	4.343	1.431	0.995	28333	438.3	0.01547
23	303.3	4.784	1332	4.809	1.431	0.995	28326	440.4	0.01555
24L	353	4.784	167.9	1.038	2.456	0.2785	398.2	170.1	0.427
24V	353	4.784	1535	5.393	0.289	0.9304	88.54	37.81	0.385
25L	381.4	15.48	265.4	1.356	3.542	0.3654	614.6	773.3	1.258
25V	381.4	15.48	1550	4.898	0.7465	0.9432	470.5	591.9	0.864
26	353	4.784	164.9	1.038	0.6287	0.2785	3514	54.41	0.01548
27	353.4	15.48	167.4	1.042	0.6287	0.2785	3515	54.57	0.01553
28	310.2	15.48	-72.65	0.3929	3.598	0.5111	36489	566.2	0.01552
29	298.2	1.012	104.8	0.3669	0.6189	-	1.546	0	0
30	333	1.012	250.7	0.8295	0.6189	-	6.444	0	0
31	298.2	1.012	104.8	0.3669	18.38	-	45.91	0	0
32	320.4	1.012	198	0.6681	18.38	-	106.8	5.618	0.05261
33	298.2	1.012	104.8	0.3669	23.11	-	57.73	0	0
34	281.2	1.012	33.97	0.1222	23.11	-	106.1	5.309	0.05004
35	298.2	1.012	104.8	0.3669	7.632	-	19.06	0	0
36	343	1.012	292.5	0.9533	7.632	-	117.1	9.986	0.08526
37	298.2	1.012	104.8	0.3669	0.01404	-	0.03507	0	0
38	353.2	1.012	335	1.075	0.01404	-	0.3009	1.513	5.027
39	353.2	1.012	119.5	0.3788	0.01644	-	3.03	0.3473	0.1146
40	353.2	1.012	335	1.075	0.003977	-	0.08524	0.114	1.337
41	353.2	1.012	335	1.075	0.01802	-	0.3861	1.626	4.212
42	353.2	1.012	4723	55.81	0.001571	-	183.4	21.02	0.1146
43	353.2	1.012	50.8	0.1566	0.01247	-	1.591	0.2333	0.1466

With consideration of the discussion above, for the presented system, the cost equation of each system's component is given in Table 2.

The heat transfer area is computed based on the Logarithmic Mean Temperature Difference (LMTD) method as follows:

$$A_k = \frac{\dot{Q}_k}{U_k \times \Delta T_{LMTD}} \tag{30}$$

$$\Delta T_{LMTD} = \frac{\Delta T_A - \Delta T_B}{ln\frac{\Delta T_A}{\Delta T_B}} \tag{31}$$

Table 3 illustrates auxiliary relations and exergy cost rate balances for the presented system components

As illustrated in Table 3, the cost per exergy unit of cooling water (c_{10}andc_{31}) are usually assumed to be zero in the energy systems powered by Sabalan (Savalan) geothermal power plant [43,48].

Finally, the Total Unit Cost of Product (TUCP) is defined as:

$$TUCP = \frac{\dot{C}_{W,net} + \dot{C}_{34} + \dot{C}_{36} + \dot{C}_{42}}{\dot{W}_{net} + \dot{E}x_{34} + \dot{E}x_{36} + \dot{E}x_{42}} \tag{32}$$

3.4. Optimization

Numerous optimization mechanisms are used in energy systems to achieve optimal performance points [61–63], but NSGA-II is the most important [64]. A random search mechanism is used in this optimization method to optimize problems, specifically time optimization [65]. NSGA-II is a popular multi-objective optimization algorithms since it has three benefits: a rapid and non-dominated sorting method, a fast crowded distance estimation procedure, and a simple crowded comparison operator [66]. To achieve optimum working conditions in thermodynamic cycles, NSGA-II is used [67]. In this way, the EES and MATLAB software is coupled to accomplish two-objective optimization for recognizing the best performance of the presented system and optimal operating conditions. Table 5 shows the five decision variables and their ranges which are assumed to optimize the presented system. Meanwhile, Fig. 2 shows the flowchart of the NSGA-II suitably.

4. Validation

The accuracy of thermodynamic simulation of the studied subsystems, namely single flash geothermal cycle, electrolyzer unit, and branched GAX cycle, is needed to be first scrutinized. To fulfill this importance, when flash cycle pressure changes between 100 kPa and 600 kPa, the power generation of the cycle is compared with that for Ref. [68]. As seen in Fig. 3(a), the obtained outcomes via this verification confirm the accuracy of modeling the single flash cycle.

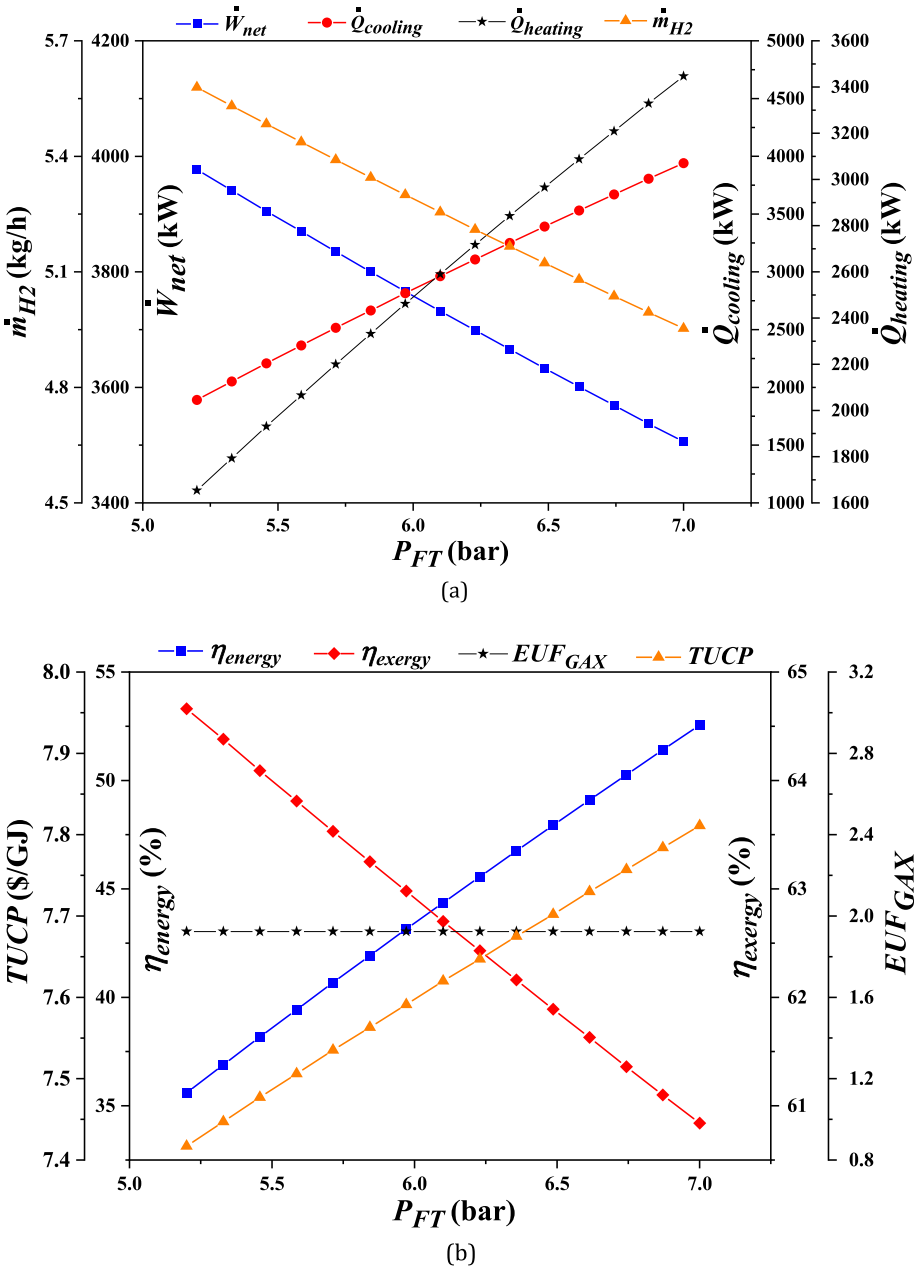

Fig. 4. (a-b): Effect of flash tank pressure on the presented system outputs.

On the other hand, as a key subsystem, the electrolyzer is validated at 80 °C, and the simulation outcomes are compared with an experimental work by Ioroi et al. [69] and are shown in Fig. 3(b).

To validate the branched GAX cycle, the obtained COP from modeling is compared with those for Refs. [70–72] in Table 4. According to Table 4, the highest relative error with 1.66% is for validation of Udayakumar [71]. It is important to note that operating conditions for all three papers are alike.

5. Results and discussion

5.1. Parametric study

Inspecting the influence of different variables on the thermodynamic system's essential outputs can provide vital views for designers in experimental projects. Taking this into consideration, the effects of evaporator temperature, generator temperature, condenser 2 temperature, flash tank pressure, and degassing value (D_x) as five design/operational parameters on net electricity, cooling and heating loads, produced hydrogen rate, energy and exergy efficiencies, Energy Utilization Factor of branched GAX cycle (EUF_{GAX}), and Total Unit Cost of Product (TUCP) for the presented system are scrutinized. Thereby, when the influence of one of the five variables on the proposed system's essential outcomes is studied, the rest of them have identical values (equal to the values in Table 5).

The input data for the presented system are given in Table 5.

To calculate the thermodynamic properties and exergoeconomic outcomes for each state of the base conditions is used input data from Table 5. Thereby, Table 6 shows these outcomes.

5.1.1. Effect of flash tank pressure on the presented system outputs

One of the critical variables in the single flash geothermal cycle is flash tank pressure, whose impacts on the eight essential outcomes of the presented system in the pressure range 5.2-7 bar are demonstrated in

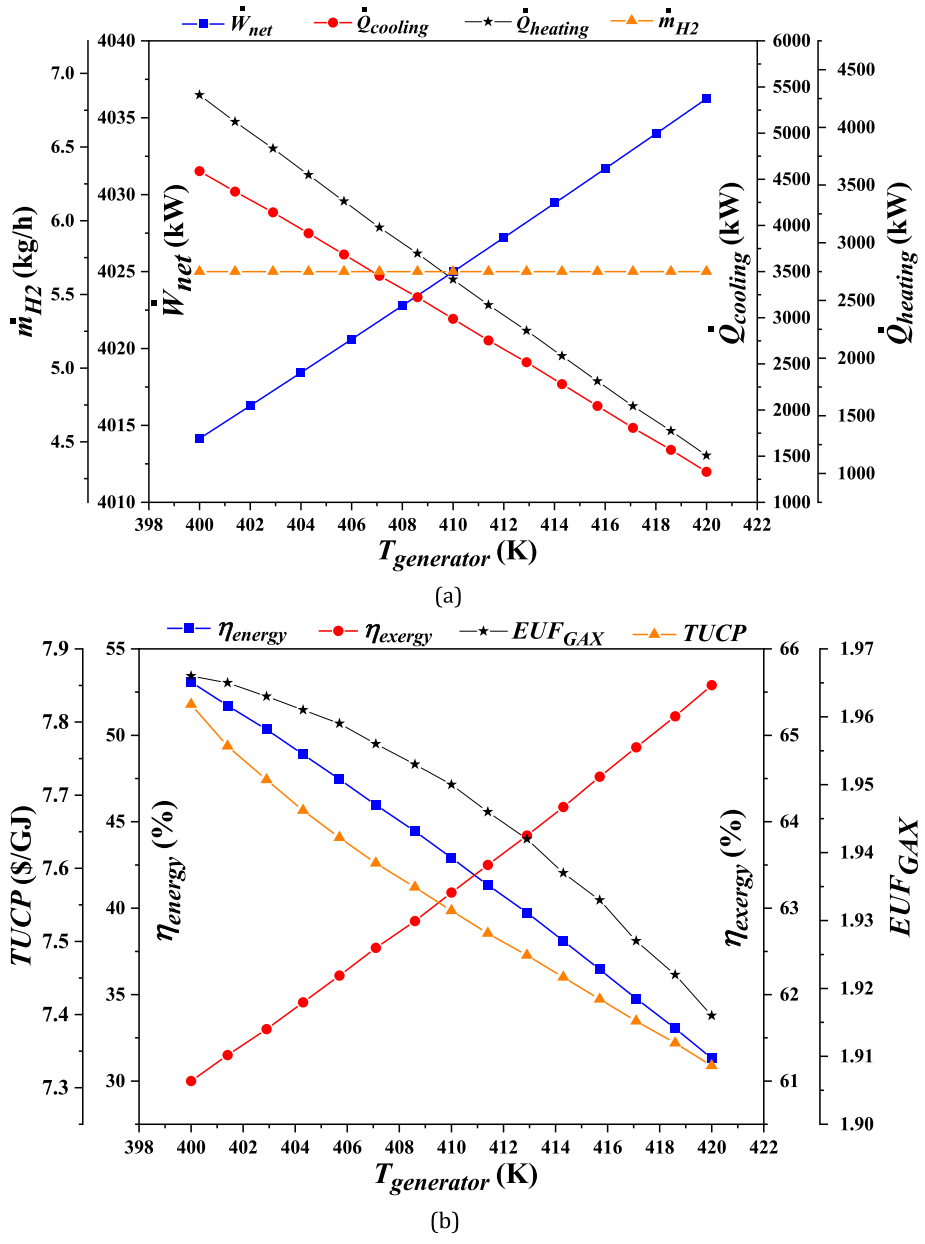

Fig. 5. (a-b): Effect of generator temperature on the presented system outputs.

Fig. 4(a-b). Notably, the most conspicuous influence of the rising pressure by passing through the constant enthalpy process (in the EV) is the decrease in the quality of the working fluid [75]. Therefore, with increasing flash tank pressure, the inlet quality in the flash tank (x_2) decreases, and consequently, $\dot{m}_3$ and $\dot{m}_7$ decrease and increase, respectively. Obviously, with increasing flash tank pressure, $\dot{m}_3$ and $\dot{W}_{tur}$ decrease. It means that increasing flash tank pressure is led to a decline in net electricity, as displayed in Fig. 4(a). It should be noted that the required electricity to run the PEME is supplied by the turbine power. It means that the produced hydrogen rate has a decreasing trend with increasing flash tank pressure. On the other hand, with raising flash tank pressure, the properties of the generator inlet (state 7) increase, resulting in an increment in mass flow rate at the branched GAX cycle, which is the logic behind the improvement of cooling and heating loads. Numerically, as can be seen in Fig. 4(a), the highest cooling and heating loads are at the flash tank pressure of 7 bar, with 3941 kW and 3447 kW, respectively. On the opposite side, the maximum produced hydrogen rate and net electricity are calculated at the flash tank pressure of 5.2 bar, with 3977 kW and 5.579 kg/h, respectively.

Despite increasing heat transfer in the generator and cooling and heating loads, due to their identical effect, the Energy Utilization Factor of the branched GAX cycle remains constant and equal to 1.924. As can be seen in Fig. 4(a), energy efficiency can rise with increasing flash tank pressure. On the contrary, exergy efficiency has a decreasing trend. Quantitatively speaking, energy and exergy efficiencies at the flash tank pressure of 7 bar are equal to 52.55% and 60.84%. From the exergoeconomic outlook, the production costs of cooling and heating loads are more dominant than the cost of the other two products, which means that TUCP rises with the increasing pressure of the flash tank. According to Fig. 4(b), numerically, the lowest TUCP is obtained at the flash tank pressure of 5.2 bar, which is equal to 7.417 $/GJ.

5.1.2. *Effect of generator temperature on the presented system outputs*

Fig. 5(a-b) depicts the trend of the presented system outputs regarding generator temperature as a variable. With the increase of generator temperature, electricity generation in the turbine remains constant. It is worth noting that the produced hydrogen rate entirely

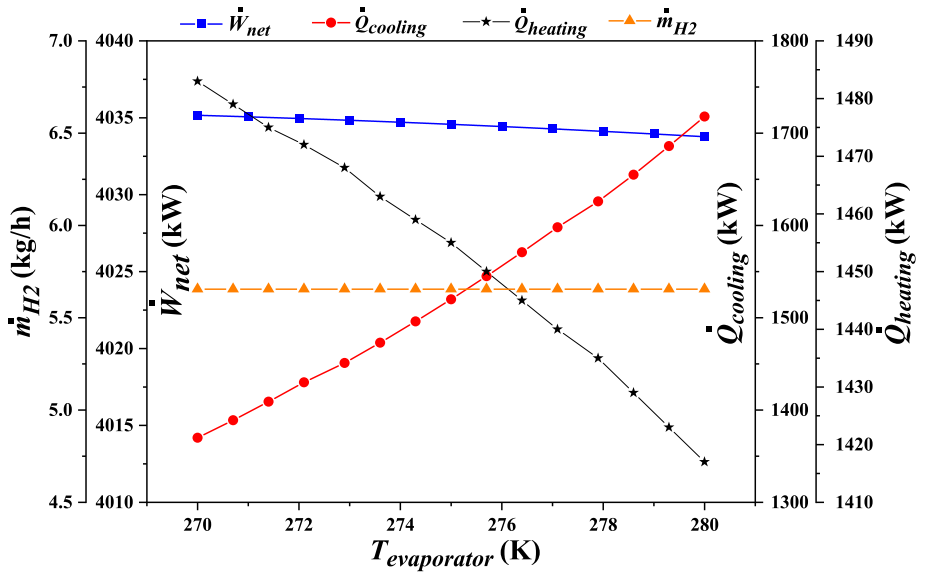

(a)

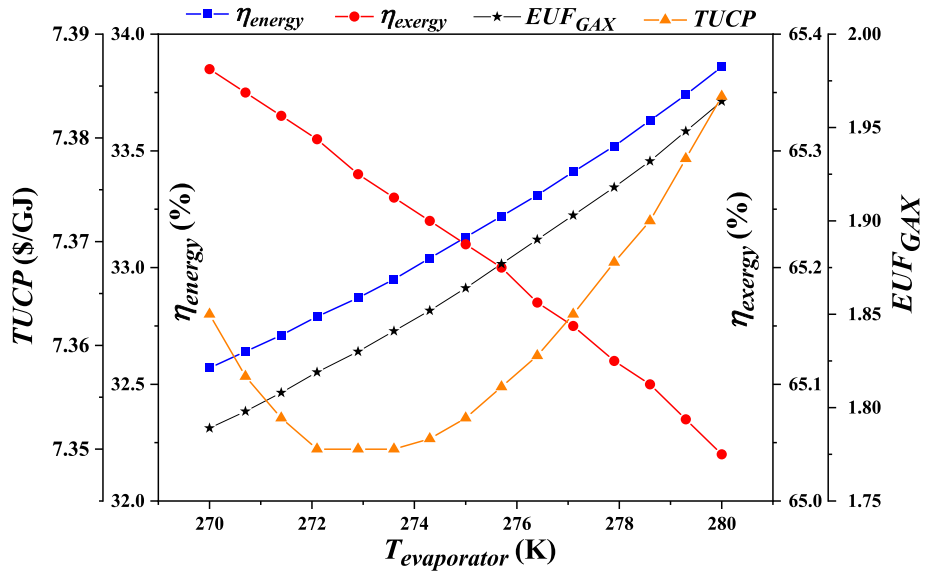

(b)

Fig. 6. (a-b): Effect of evaporator temperature on the presented system outputs.

depends on electricity generation in the turbine. Thus, the produced hydrogen rate does not have any changes. On the other hand, decreasing mass flow rate in the branched GAX subsystem occurs by increasing the generator temperature. It means that the consumption of power in pumps 2 and 3 and cooling and heating loads is reduced. That is why the net electricity has an increasing trend with an increment of the generator temperature. Numerically, as can be seen in Fig. 5(a), the highest cooling and heating loads are obtained at the generator temperature of 400 K, with 4588 kW and 4281 kW, respectively. On the opposite side, the maximum net electricity is calculated at the generator temperature of 420 K, with 4036 kW.

When the heat transferred to the presented system is constant and loads of cooling and heating fall, the energy efficiency and Energy Utilization Factor of the branched GAX cycle see a reduction by rising the generator temperature. However, the exergy efficiency entirely depends on net electricity, and that is why it has an increasing trend. According to Fig. 5(b), numerically, at the generator temperature of 400 K, the highest energy efficiency and Energy Utilization Factor of the branched GAX cycle are obtained, with 53.08% and 1.966, respectively. In contrast, the maximum exergy efficiency is achieved at the generator temperature of 420 K with 65.58%. TUCP has a decreasing trend with an increment of generator temperature due to reducing system productions such as cooling and heating loads, which have an impressive influence on the presented system costs. Quantitatively speaking, minimum TUCP is obtained at the generator temperature of 420 K, with 7.33 $/GJ.

5.1.3. *Effect of evaporator temperature on the presented system outputs*

The effects of evaporator temperature on system outcomes are displayed in Fig. 6(a-b). Similar to the generator temperature, with the increasing evaporator temperature, electricity generation in the turbine and produced hydrogen rate remain constant, while the mass flow rate passing through the branched GAX cycle increases and causes an increment in cooling load. Net electricity and heating load are reduced by an increment of evaporator temperature. Therefore, when the evaporator temperature goes up from 270 K to 280 K, the cooling load increases from 1251 kW to 1718 kW, while heating load and net

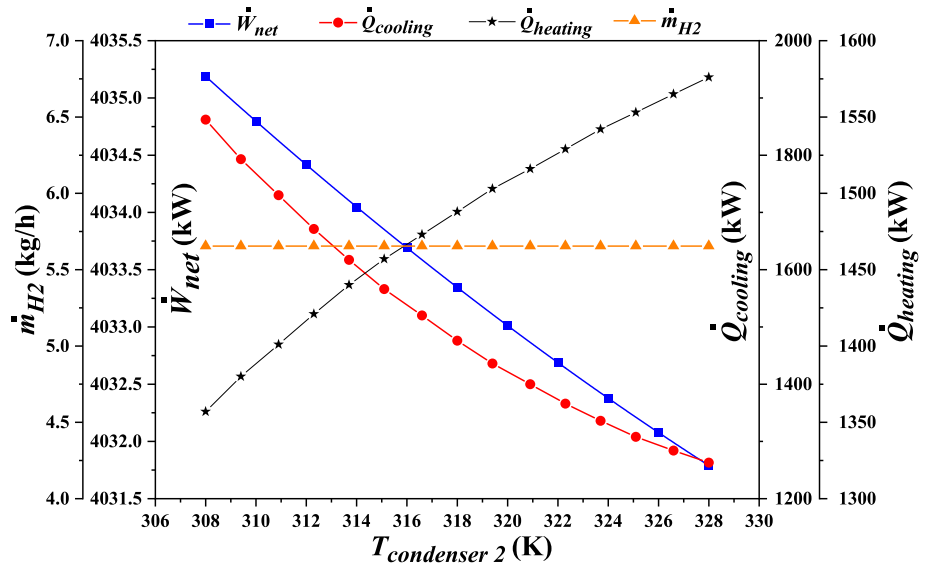

(a)

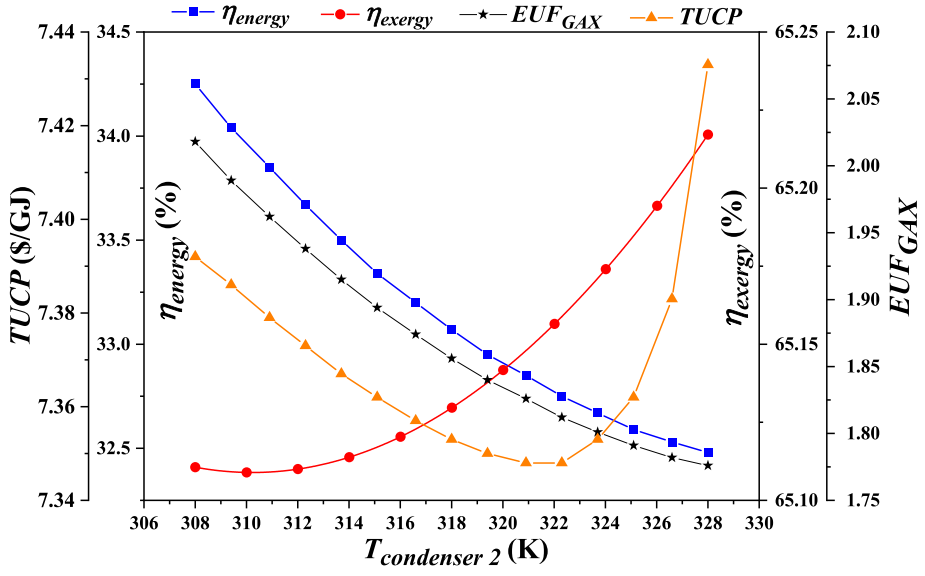

(b)

Fig. 7. (a-b): Effect of condenser 2 temperature on the presented system outputs.

electricity fall from 1504 kW to 1417 kW and from 4036 kW to 4034 kW, respectively.

As can be seen in Fig. 6(a), with increasing evaporator temperature, increasing the cooling load has a keener trend in comparison with the reduction of net electricity and heating load. Therefore, having constant heat input, energy efficiency and Energy Utilization Factor of the branched GAX cycle go up by the rising evaporator temperature. According to Fig. 6(b), at the evaporator temperature of 280 K, the highest values for energy efficiency and Energy Utilization Factor of the branched GAX cycle obtain as 33.86% and 1.964, whereas their minimum values are equal to 32.12% and 1.729 at the evaporator temperature of 270 K, respectively. Moreover, at the evaporator temperature of 270 K and 280 K, the highest and lowest exergy efficiencies are 66.01% and 65.04%, respectively. Interestingly, TUCP has a minimum value at the evaporator temperature of 273 K, which may be caused by the opposite trend between the cost of cooling load and the costs of net electricity and heating load. As a quantitative outcome, the lowest TUCP is equal to 7.35 $/GJ.

5.1.4. Effect of condenser 2 temperature on the presented system outputs

The influence of condenser 2 temperature on the key presented system outputs is displayed in Fig. 7(a-b). As previous variables (i.e., temperatures of generator and evaporator), electricity generation in the turbine and produced hydrogen rate remain intact. Also, raising the temperature of condenser 2 from 308 K to 328 K has a reverse effect on net electricity and cooling load and causes a decrement in cooling load and net electricity. It is important to note that the total heat transfer in the absorber is the aggregate of the heating load and available heat transfer in the absorber. By increasing condenser 2 temperature, the available heat transfer in the absorber is reduced and leads to the heating load enhancement, and numerically, when the condenser 2 temperature grows up from 308 K to 328 K, the heating load boosts from 1357 kW to 1576 kW. According to Fig. 7(a), the highest net electricity and cooling load are achieved when the condenser 2 temperature is 308 K, with 4035 kW and 1862 kW, respectively.

It is worth mentioning that the produced hydrogen rate is constant with the increasing temperature of condenser 2, while the heat input to the presented system decreases. As can be seen in Fig. 7(a), the

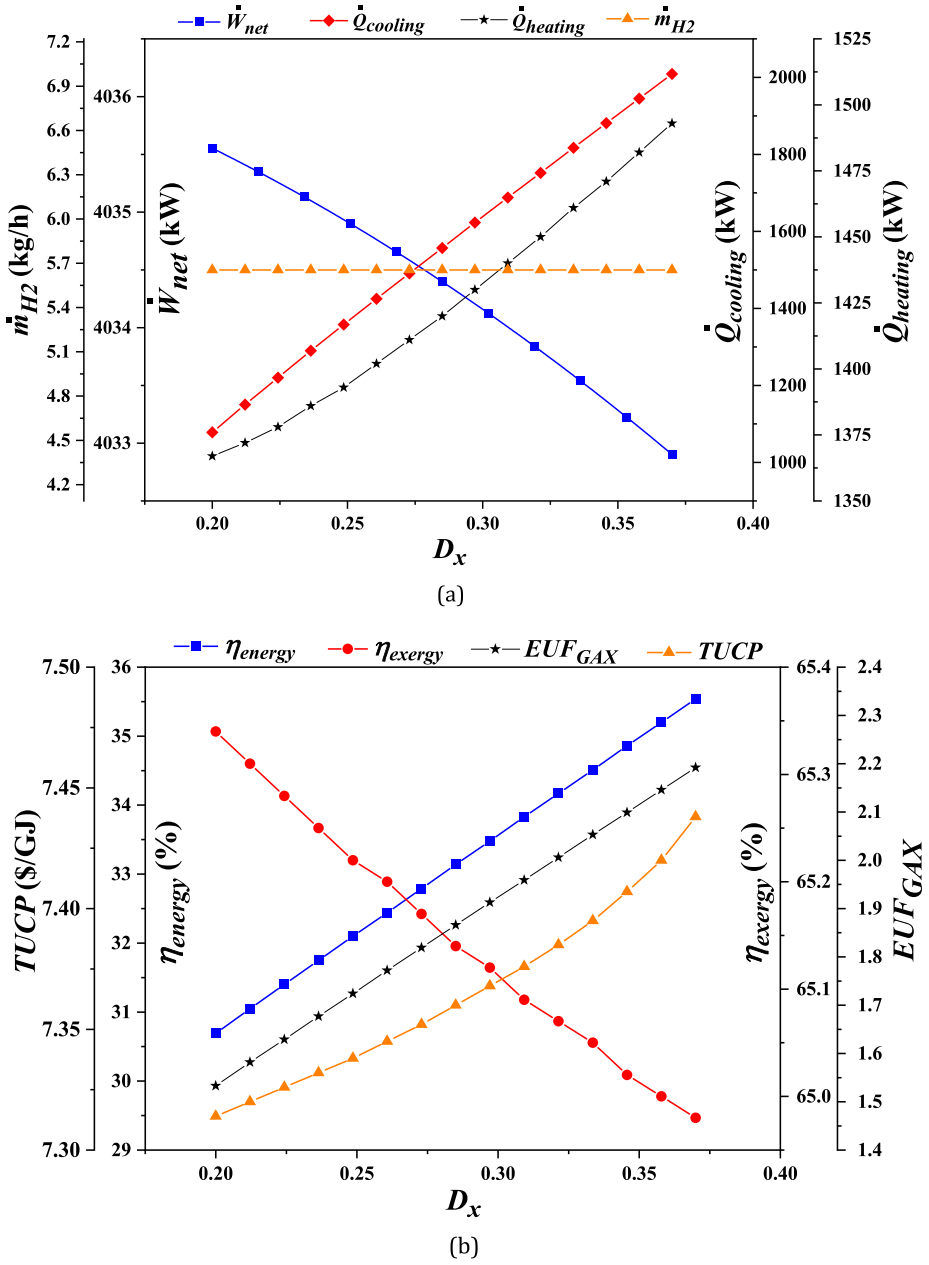

Fig. 8. (a-b): Effect of degassing value on the presented system outputs.

decreasing trend of cooling load and net electricity is more dominant than the increasing heating load and leads to decreasing energy efficiency and Energy Utilization Factor of the branched GAX cycle, as shown in Fig. 7(b). Notwithstanding reducing net electricity, exergy efficiency increases slightly, which is due to more reduction of input exergy. Quantitively speaking, when condenser 2 temperature goes up from 308 K to 328 K, exergy efficiency rises from 65.11% to 65.22%, while energy efficiency decreases from 34.25% to 32.48%. Fig. 7(b) reveals that the TUCP has a minimum value at the condenser 2 temperature of 322.3 K, which equals 7.348 $/GJ.

5.1.5. Effect of degassing value on the presented system outputs

The effect of degassing value on the key presented system outputs is shown in Fig. 8(a-b). Degassing value is one of the most important variables to investigate the proposed system based on the branched GAX cycle, which is defined as the difference in concentration between rich and weak solutions. Similar to the previous variable, electricity generation in the turbine and produced hydrogen rate remain unchanged, in which the produced hydrogen rate is equal to 5.655 kg/h, as shown in Fig. 8(a). The increment of degassing value means that the passed mass flow rate through the evaporator, absorber, pump 2, and pump 3 increases, while the mass flow rate passing the generator does not have any changes, which leads to an increasing trend for heating and cooling loads and decreasing trend for net electricity. Numerically, when the degassing value goes up from 0.2 to 0.37, cooling and heating loads rise by 86.36% and 9.22%, and the net electricity is reduced to 4033 kW.

Based on Eq. (21), the Energy Utilization Factor of the branched GAX cycle entirely depends on cooling and heating loads. Referring to Fig. 8 (a), these outputs have an increasing trend with an increment of degassing value and lead to an increased Energy Utilization Factor of the branched GAX cycle from 1.533 to 2.192. Also, the energy efficiency has a behavior similar to the mentioned output and can grow from 30.69% to 35.54%. On the contrary, exergy efficiency is slightly reduced with increasing degassing value. From the exergoeconomic viewpoint, the production costs of cooling and heating loads are more dominant than the cost of the other two products, which means that TUCP rises with an

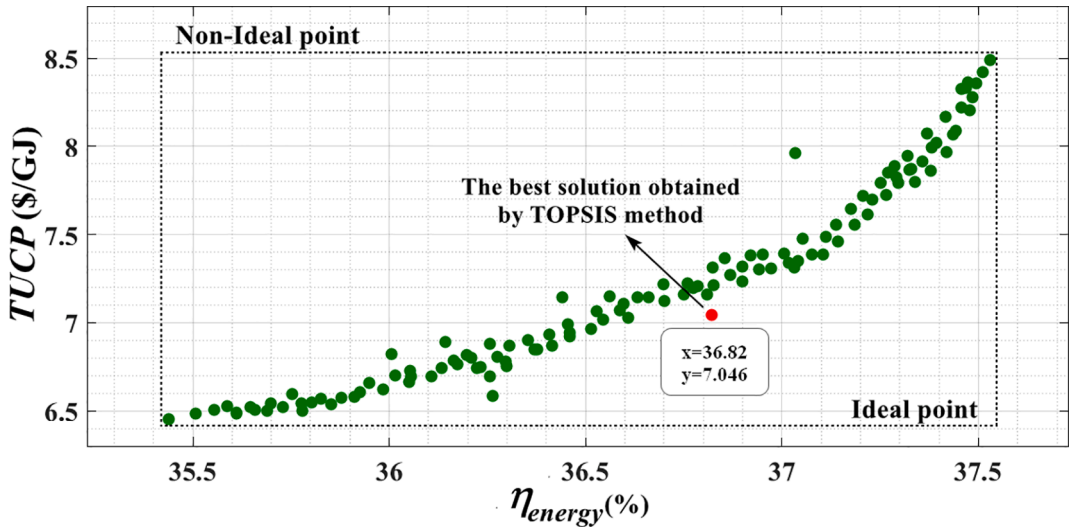

Fig. 9. Pareto optimal frontier obtained by two-objective optimization.

Table 7
Decision variables and main outcomes of the proposed system.

Parameters	Base mode	Optimal mode
Decision variables		
Flash tank working pressure, P_{FT} (bar)	5.2	5.58
Evaporator temperature, T_{eva} (K)	278	265.3
Condenser 2 temperature, T_{cond2} (K)	313	326
Generator temperature, T_{gen} (K)	418	418.5
Degassing value, D_x	0.30	0.357
Main outcomes		
Produced hydrogen rate,$\dot{m}_{42}$(kg/h)	5.65	5.44
Heating load,$\dot{Q}_{heating}$ (kW)	1638	2122
Cooling load,$\dot{Q}_{cooling}$ (kW)	1432	1658
Net electricity,$\dot{W}_{net}$ (kW)	4034	3878
Energy efficiency,η_{energy}(%)	33.56	36.82
Exergy efficiency,η_{exergy}(%)	65.11	65.42
Overall exergy fuel rate,$\dot{E}x_F^{total}$(kW)	6702	6610
Overall exergy production rate,$\dot{E}x_P^{total}$(kW)	4364	4324
Overall exergy loss rate,$\dot{E}x_L^{total}$(kW)	192.1	203.7
Overall exergy destruction rate,$\dot{E}x_D^{total}$(kW)	2146	2082
Overall investment cost rate,$\dot{Z}_{total}$($/h)	123	25.57
Overall cost rate of exergy destruction,$\dot{C}_D^{total}$ ($/h)	8.25	23.99
Overall cost rate of exergy loss rate,$\dot{C}_L^{total}$($/h)	32.96	109.7
Overall cost rate of exergy fuel rate,$\dot{C}_F^{total}$($/h)	25.77	8.05
Overall cost rate of exergy production rate,$\dot{C}_P^{total}$($/h)	115.8	108.1
Total unit cost of product, *TUCP*($/GJ)	7.37	7.046

increment of degassing value. According to Fig. 8(b), numerically, the lowest and highest TUCP are obtained at degassing values of 0.2 and 0.37, which are equal to 7.314 $/GJ and 7.438, respectively.

5.2. Optimization results

The objectives should be conflicting in two-objective optimization. In light of this, the two-objective optimization is taken energy efficiency and TCUP into account. Multi-objective optimization leads to the Pareto frontier. Fig. 9 illustrates the related Pareto frontier. The technique for order of preference by similarity ideal solution (TOPSIS) is one of the decision-making approaches [32,76]. It is used in this study to select the best optimal solution attained from the NSGA-II multi-objective optimization. The distance between the ideal solution and other solutions on the Pareto frontier and also the distance between the non-ideal solution and other solutions are considered as the main terms to specify the final optimal solution. In this regard, optimum values are 7.046 $/GJ and 36.82% for TUCP and energy efficiency.

Calculation of the outcomes of two-objective optimization and comparing them with the obtained outcomes of the base case can provide a helpful signal for designers to demonstrate the importance of optimization effects and determine the intended working conditions. Owing to this, Table 7 indicates the presented system outputs in the base and optimized conditions. Outcomes show that values of produced hydrogen rate, net electricity, and overall exergy production rate in the base case are more than optimal mode, which are equal to 5.65 kg/h, 4034 kW, and 4364 kW, respectively. However, the TUCP of the proposed system in the optimal mode is smaller than in the base case. Also, high cooling and heating loads and energy and exergy efficiencies are obtained in the optimal mode, which are equal to 1658 kW, 2122 kW, 36.82%, and 65.42%, respectively.

Exergy destruction rate related to apiece component is an imperative output in exergy investigation. Accordingly, estimating this outcome and finding solutions to decrease it should be taken into account in the new system's design. Fig. 10 illustrates the exergy flow diagram in optimum conditions. As can be seen in Fig. 10, the total input exergy to the presented system is equal to 6601 kW, of which the overall exergy production rate, overall exergy destruction rate, and overall exergy loss rate are equal to 4324 kW (65.42% of total input exergy), 2082 kW (31.50% of total input exergy), and 203.7 kW (3.08% of total input exergy), respectively. The exergy production rate of electricity with 3878 kW (58.67% of total input exergy) is more than other exergy productions. Moreover, the highest exergy rate destruction occurs in the turbine, which is equal to 746.4 kW (11.29% of total input exergy).

5.3. Comparison with SGPP-based multi-generation systems

In previous studies, many researchers have used existing data for SGPP to propose and scrutinize new multi-generation systems. Thermodynamic and thermoeconomic approaches are used mainly to examine these systems. In most cases, producing cooling in such systems has not been paid attention to; indeed, the main aim of the proposing SGPP-based systems is electricity generation. Meanwhile, cooling production next to the producing electricity, heating, and hydrogen is more important due to climate change and global warming. Thanks to the more ability of the branched GAX cycle to produce cooling and the ability to operate by a heat source temperature over 150 °C, it can be used as a subsystem of SGPP. Owing to this, in this section, key outcomes of the proposed system are compared with the proposed system by Cao et al. [77]. Their offered system is based on the SGPP and is able to

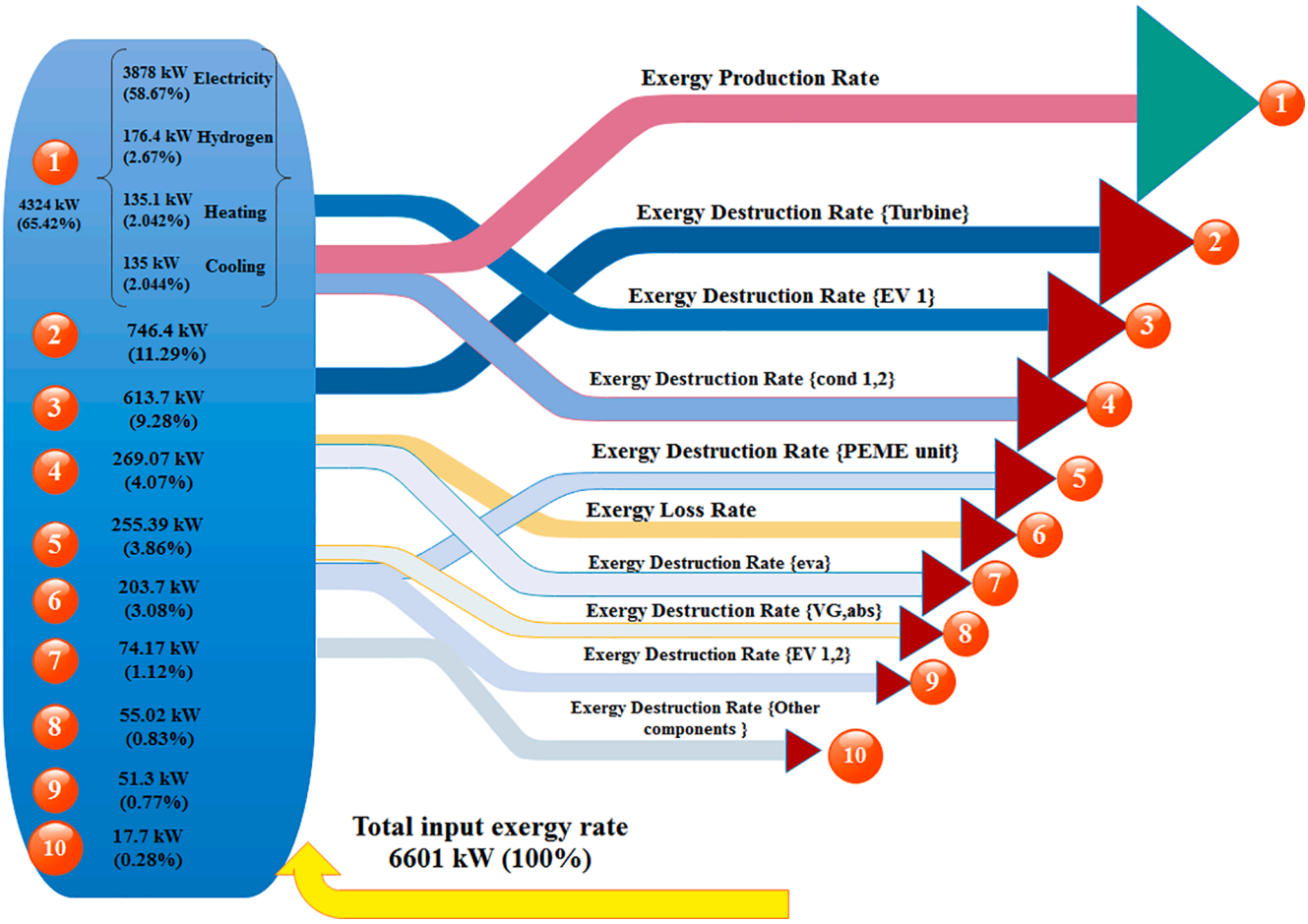

Fig. 10. Exergy flow diagram of the multi-generation system at optimum conditions.

Table 8
Comparing key outcomes of the proposed system with work by Cao et al. [77].

Parameters	Work by Cao et al. [77]	Current study
Operating conditions		
Pressure of geothermal water, $P_1\,(bar)$	12	12
Enthalpy of geothermal water, $h_1\,(kJ/kg)$	1000	1000
Mass flow rate of geothermal water, $\dot{m}_1\,(kg/s)$	45	45
Flash tank pressure, $P_{FT}\,(bar)$	5.5	5.5
Turbine expansion ratio, ER_{tur}	120	120
Turbine isentropic efficiency, $\eta_{is.tur}$ (%)	85	85
Pump isentropic efficiency, $\eta_{is.pu}$ (%)	85	85
PEME temperature, T_{PEME} (K)	353	353
Unit cost of geofluid exergy, $C_1\,(\$/GJ)$	1.3	1.3
Key outcomes		
Produced hydrogen rate, $\dot{m}_{H2}\,(kg/h)$	4.52	5.47
Freshwater production rate, $\dot{m}_{FW}\,(m^3/h)$	97.62	-
Heating load, $\dot{Q}_{heating}\,(kW)$	-	2260
Cooling load, $\dot{Q}_{cooling}\,(kW)$	-	1976
Net electricity, $\dot{W}_{net}\,(kW)$	4310	3893
Energy efficiency, η_{energy} (%)	14.00	38.59
Exergy efficiency, η_{exergy} (%)	46.09	64.00
Overall exergy destruction rate, $\dot{E}x_D^{total}\,(kW)$	4341	2197
Overall investment cost rate, $\dot{Z}_{total}\,(\$/h)$	196.4	114.1
Overall cost rate of exergy destruction, $\dot{C}_D^{total}$ $(\$/h)$	20.18	8.5
Total unit cost of product, $TUCP(\$/GJ)$	8.15	7.486

produce electricity and fresh water. Table 8 shows the results of the comparison with similar operating conditions. As can be seen in Table 8, the number of the products in this study is more than the proposed system by Cao et al. [77], which is led to reaching high energy and exergy efficiencies and low TUCP. The energy efficiency of the current study is equal to 38.59%, while this value in the Ref. [77] is 14%. Moreover, exergy efficiency is 17.91%-points higher than the Ref. [77]. As illustrated in Table 8, values of overall exergy destruction rate, overall investment cost rate, overall cost rate of exergy destruction, and Total Unit Cost of Product in the current study obtain as 2197 kW, 114.1 $/h, 8.5 $/h, and 7.486 $/GJ, while these values in work by Cao et al. [77] are equal to 4341 kW, 196.4 $/h, 20.18 $/h, and 8.15 $/GJ, respectively.

6. Conclusions

A novel multi-generation system powered by Sabalan (Savalan) geothermal power plant is proposed based on the single flash cycle, a branched GAX cycle, and an electrolyzer, which is able to generate electricity, hydrogen, heating, and cooling. The main thermodynamic, exergoeconomic, and optimization outcomes can be summarized as:

- Produced hydrogen rate remains unchanged at 5.655 kg/h by variation of the temperature of the generator, condenser 2, and evaporator as well as degassing value.
- By increasing flash tank pressure from 5.2 bar to 7 bar, the cooling and heating loads improve about 108.4%, while the net electricity falls from 3977 kW to 3506 kW.

- TUCP has a minimum value at the condenser 2 temperature of 322.3 K and evaporator temperature of 273 K.
- The optimal values are 7.046 $/GJ and 36.82% for TUCP and energy efficiency.
- At the optimum conditions, the total input exergy to the presented system is equal to 6601 kW, of which the overall exergy production rate, overall exergy destruction rate, and overall exergy loss rate are equal to 4324 kW (65.42% of total input exergy), 2082 kW (31.50% of total input exergy), and 203.7 kW (3.08% of total input exergy), respectively.

CRediT authorship contribution statement

Miryasin Seiiedhoseiny: Investigation, Writing – Original draft. **Leyla Khani:** Conceptualization, Reviewing and Editing. **Mousa Mohammadpourfard:** Supervision, Reviewing and Editing. **Gülden G. Akkurt:** Reviewing and Editing.

Declaration of Competing Interest

The authors declare that they have no known competing financial interests or personal relationships that could have appeared to influence the work reported in this paper.

Data availability

No data was used for the research described in the article.

References

[1] Khani L, Mohammadpour M, Mohammadpourfard M, Heris SZ, Akkurt GG. Thermodynamic design, evaluation, and optimization of a novel quadruple generation system combined of a fuel cell, an absorption refrigeration cycle, and an electrolyzer. Intl J of Energy Res 2022;46(6):7261–76.

[2] Taheri MH, Khani L, Mohammadpourfard M, Aminfar H. Multi-objective optimization of a novel biomass-based multigeneration system consisting of liquid natural gas open cycle and proton exchange membrane electrolyzer. Int J Energy Res 2021;45:16806–23. doi: 10.1002/er.6931.

[3] Deymi-Dashtebayaz M, Rezapour M, Farahnak M. Modeling of a novel nanofluid-based concentrated photovoltaic thermal system coupled with a heat pump cycle (CPVT-HP). Appl Therm Eng 2022;201:117765. https://doi.org/10.1016/j.applthermaleng.2021.117765.

[4] Zhu D, Wang B, Ma H, Wang H. Evaluating the vulnerability of integrated electricity-heat-gas systems based on the high-dimensional random matrix theory. CSEE J Power Energy Syst 2020;6:878–89. https://doi.org/10.17775/CSEEJPES.2019.00440.

[5] Nazerifard R, Khani L, Mohammadpourfard M, Mohammadi-Ivatloo B, Akkurt GG. Design and thermodynamic analysis of a novel methanol, hydrogen, and power trigeneration system based on renewable energy and flue gas carbon dioxide. Energy Convers Manag 2021;233:113922. https://doi.org/10.1016/j.enconman.2021.113922.

[6] Khani L, Jabari F, Mohammadpourfard M, Mohammadi-ivatloo B. Design, evaluation, and optimization of an efficient solar-based multi-generation system with an energy storage option for Iran's summer peak demand. Energy Convers Manag 2021;242:114324. https://doi.org/10.1016/j.enconman.2021.114324.

[7] Parikhani T, Azariyan H, Behrad R, Ghaebi H, Jannatkhah J. Thermodynamic and thermoeconomic analysis of a novel ammonia-water mixture combined cooling, heating, and power (CCHP) cycle. Renew Energy 2020;145:1158–75. https://doi.org/10.1016/j.renene.2019.06.100.

[8] Azariyan H, Vajdi M, Rostamnejad TH. Assessment of a high-performance geothermal-based multigeneration system for production of power, cooling, and hydrogen: Thermodynamic and exergoeconomic evaluation. Energy Convers Manag 2021;236:113970. https://doi.org/10.1016/j.enconman.2021.113970.

[9] Li Y, Yang Y. Thermodynamic analysis of a novel integrated solar combined cycle. Appl Energy 2014;122:133–42. https://doi.org/10.1016/j.apenergy.2014.02.017.

[10] McClure S. Unlocking Japan's geothermal energy potential | the Japan Times. The Japan Times 2019. https://doi.org/https://www.japantimes.co.jp/life/2019/03/09/environment/unlocking-japans-geothermal-energy-potential/#.XSmVfOgzbIU.

[11] Hekmatshoar M, Deymi-Dashtebayaz M, Gholizadeh M, Dadpour D, Delpisheh M. Thermoeconomic analysis and optimization of a geothermal-driven multi-generation system producing power, freshwater, and hydrogen. Energy 2022;247:123434. https://doi.org/10.1016/j.energy.2022.123434.

[12] Cengel YA, Boles MA, Kanoğlu M. Thermodynamics: an engineering approach, vol. 5. McGraw-hill New York; 2011.

[13] Kanoğlu M, Çengel YA. Economic evaluation of geothermal power generation, heating, and cooling. Energy 1999;24:501–9. https://doi.org/10.1016/S0360-5442(99)00016-X.

[14] Nami H, Anvari-Moghaddam A. Geothermal driven micro-CCHP for domestic application – Exergy, economic and sustainability analysis. Energy 2020;207:118195. https://doi.org/10.1016/j.energy.2020.118195.

[15] Ambriz-Díaz VM, Rubio-Maya C, Ruiz-Casanova E, Martínez-Patiño J, Pastor-Martínez E. Advanced exergy and exergoeconomic analysis for a polygeneration plant operating in geothermal cascade. Energy Convers Manag 2020;203:112227. https://doi.org/10.1016/j.enconman.2019.112227.

[16] Parikhani T, Gholizadeh T, Ghaebi H, Sattari Sadat SM, Sarabi M. Exergoeconomic optimization of a novel multigeneration system driven by geothermal heat source and liquefied natural gas cold energy recovery. J Clean Prod 2019;209:550–71. https://doi.org/10.1016/j.jclepro.2018.09.181.

[17] Zare V, Takleh HR. Novel geothermal driven CCHP systems integrating ejector transcritical CO 2 and Rankine cycles : thermodynamic modeling and parametric study. Energy Convers Manag 2020;205:112396. https://doi.org/10.1016/j.enconman.2019.112396.

[18] Takleh HR, Zare V. Proposal and thermoeconomic evaluation with reliability considerations of geothermal driven trigeneration systems with independent operations for summer and winter. Int J Refrig 2021;127:34–46.

[19] Gnaifaid H, Ozcan H. Development and multiobjective optimization of an integrated flash-binary geothermal power plant with reverse osmosis desalination and absorption refrigeration for multi-generation. Geothermics 2021;89:101949. https://doi.org/10.1016/j.geothermics.2020.101949.

[20] Ansari SA, Kazim M, Khaliq MA, Abdul Hussain Ratlamwala T. Thermal analysis of multigeneration system using geothermal energy as its main power source. International Journal of Hydrogen Energy 2021;46(6):4724–38.

[21] Liu L, Meng X, Miao Z, Zhou S. Design of a novel thermoelectric module based on application stability and power generation. Case Stud Therm Eng 2022;31:101836. https://doi.org/10.1016/j.csite.2022.101836.

[22] Miao Z, Meng X, Liu L. Analyzing and optimizing the power generation performance of thermoelectric generators based on an industrial environment. J Power Sources 2022;541:231699. https://doi.org/10.1016/j.jpowsour.2022.231699.

[23] Rostamnejad Takleh H, Zare V. Employing thermoelectric generator and booster compressor for performance improvement of a geothermal driven combined power and ejector-refrigeration cycle. Energy Convers Manag 2019;186:120–30. https://doi.org/10.1016/j.enconman.2019.02.047.

[24] Ali S, Sørensen K, Nielsen MP. Modeling a novel combined solid oxide electrolysis cell (SOEC) - Biomass gasi fi cation renewable methanol production system. Renew Energy 2020;154:1025–34. https://doi.org/10.1016/j.renene.2019.12.108.

[25] Hernández-Gómez Á, Ramirez V, Guilbert D, Saldivar B. Cell voltage static-dynamic modeling of a PEM electrolyzer based on adaptive parameters: Development and experimental validation. Renew Energy 2021;163:1508–22. https://doi.org/10.1016/j.renene.2020.09.106.

[26] Demir ME, Dincer I. ScienceDirect Development of a hybrid solar thermal system with TEG and PEM electrolyzer for hydrogen and power production. Int J Hydrogen Energy 2017;42(51):30044–56.

[27] Nami H, Akrami E. Analysis of a gas turbine based hybrid system by utilizing energy, exergy and exergoeconomic methodologies for steam, power and hydrogen production. Energy Convers Manag 2017;143:326–37. https://doi.org/10.1016/j.enconman.2017.04.020.

[28] Ahmadi F, Chavoshi M, Sabeti V. Multi-generation system incorporated with PEM electrolyzer and dual ORC based on biomass gasification waste heat recovery: exergetic, economic and environmental impact optimizations. Energy 2018;145:38–51. https://doi.org/10.1016/j.energy.2017.12.118.

[29] Cao L, Lou J, Wang J, Dai Y. Exergy analysis and optimization of a combined cooling and power system driven by geothermal energy for ice-making and hydrogen production. Energy Convers Manag 2018;174:886–96. https://doi.org/10.1016/j.enconman.2018.08.067.

[30] Feili M, Rostamzadeh H, Ghaebi H. Thermo-mechanical energy level approach integrated with exergoeconomic optimization for realistic cost evaluation of a novel micro-CCHP system. Renew. Energy 2022;190:630–57.

[31] Cao Y, Dhahad HA, Togun H, Hussen HM, Anqi AE, Farouk N, et al. Effect of working fluids in a novel geothermal-based integration of organic-flash and power/cooling generation cycles with hydrogen and freshwater production units. Int J Hydrogen Energy 2021;46(56):28370–86.

[32] Wang M, Yu H, Jing R, Liu H, Chen P, Li C. Combined multi-objective optimization and robustness analysis framework for building integrated energy system under uncertainty. Energy Convers Manag 2020;208:112589. https://doi.org/10.1016/j.enconman.2020.112589.

[33] Zhou Y, Li S, Sun L, Zhao S, Ashraf Talesh SS. Optimization and thermodynamic performance analysis of a power generation system based on geothermal flash and dual-pressure evaporation organic Rankine cycles using zeotropic mixtures. Energy 2020;194:116785. https://doi.org/10.1016/j.energy.2019.116785.

[34] Jawahar CP, Saravanan R. Generator absorber heat exchange based absorption cycle—a review. Renew Sustain Energy Rev 2010;14:2372–82. https://doi.org/10.1016/j.rser.2010.05.002.

[35] Mehr AS, Zare V. Energy and exergy analysis of a novel multi-generation system producing cooling, heating, power and pure water. Int J Exergy 2014;15:233–55. https://doi.org/https://www.inderscienceonline.com/doi/pdf/10.1504/IJEX.2014.065642.

[36] Mohammadi K, Saghafifar M, McGowan JG, Powell K. Thermo-economic analysis of a novel hybrid multigeneration system based on an integrated triple effect refrigeration system for production of power and refrigeration. J Clean Prod 2019;238:117912. https://doi.org/10.1016/j.jclepro.2019.117912.

[37] Pourpasha H, Mohammadfam Y, Khani L, Mohammadpourfard M, Zeinali HS. Thermodynamic and thermoeconomic analyses of a new dual-loop organic Rankine

– Generator absorber heat exchanger power and cooling cogeneration system. Energy Convers Manag 2020;224:113356. https://doi.org/10.1016/j.enconman.2020.113356.
[38] Feili M, Rostamzadeh H, Ghaebi H. A new high-efficient cooling/power cogeneration system based on a double-flash geothermal power plant and a novel zeotropic bi-evaporator ejector refrigeration cycle. Renew Energy 2020;162:2126–52. https://doi.org/10.1016/j.renene.2020.10.011.
[39] Li K, Ding Y-Z, Ai C, Sun H, Xu Y-P, Nedaei N. Multi-objective optimization and multi-aspect analysis of an innovative geothermal-based multi-generation energy system for power, cooling, hydrogen, and freshwater production. Energy 2022;245:123198. https://doi.org/10.1016/j.energy.2022.123198.
[40] Zhou Z, Cao Y, Anqi AE, Zoghi M, Habibi H, Rajhi AA, et al. Converting a geothermal-driven steam flash cycle into a high-performance polygeneration system by waste heat recovery: 3E analysis and Genetic-Fgoalattain optimization. Renew Energy 2022;186:609–27. https://doi.org/10.1016/j.renene.2022.01.009.
[41] Liu Z, Yang X, Liu Xu, Yu Z, chen Y. Performance assessment of a novel combined heating and power system based on transcritical CO2 power and heat pump cycles using geothermal energy. Energy Conversion and Management 2020;224:113355.
[42] Parikhani T, Delpisheh M, Haghghi MA, Holagh SG, Athari H. Performance enhancement and multi-objective optimization of a double-flash binary geothermal power plant. Energy Nexus 2021;2:100012. https://doi.org/10.1016/j.nexus.2021.100012.
[43] Abdolalipouradl M, Khalilarya S, Jafarmadar S. Exergoeconomic analysis of a novel integrated transcritical CO2 and Kalina 11 cycles from Sabalan geothermal power plant. Energy Convers Manag 2019;195:420–35. https://doi.org/10.1016/j.enconman.2019.05.027.
[44] Cao Y, Xu D, Togun H, Dhahad HA, Azariyan H, Farouk N. Feasibility analysis and capability characterization of a novel hybrid flash-binary geothermal power plant and trigeneration system through a case study. Int J Hydrogen Energy 2021;46:26241–62. https://doi.org/10.1016/j.ijhydene.2021.05.146.
[45] Feili M, Rostamzadeh H, Parikhani T, Ghaebi H. Hydrogen extraction from a new integrated trigeneration system working with zeotropic mixture, using waste heat of a marine diesel engine. Int J Hydrogen Energy 2020;45:21969–94. https://doi.org/10.1016/j.ijhydene.2020.05.208.
[46] Ghaebi H, Farhang B, Parikhani T, Rostamzadeh H. Energy, exergy and exergoeconomic analysis of a cogeneration system for power and hydrogen production purpose based on TRR method and using low grade geothermal source. Geothermics 2018;71:132–45. https://doi.org/10.1016/j.geothermics.2017.08.011.
[47] Rostamnejad Takleh H, Zare V, Mohammadkhani F, Sadeghiazad MM. Proposal and thermoeconomic assessment of an efficient booster-assisted CCHP system based on solar-geothermal energy. Energy 2022;246:123360. https://doi.org/10.1016/j.energy.2022.123360.
[48] Aali A, Pourmahmoud N, Zare V. Exergoeconomic analysis and multi-objective optimization of a novel combined flash-binary cycle for Sabalan geothermal power plant in Iran. Energy Convers Manag 2017;143:377–90. https://doi.org/10.1016/j.enconman.2017.04.025.
[49] Shi Y, Wang Q, Hong D, Chen G. Thermodynamic analysis of a novel GAX absorption refrigeration cycle. Int J Hydrogen Energy 2017;42:4540–7. https://doi.org/10.1016/j.ijhydene.2016.10.155.
[50] Li H, Tao Y, Zhang Y, Fu H. Two-objective optimization of a hybrid solar-geothermal system with thermal energy storage for power, hydrogen and freshwater production based on transcritical CO2 cycle. Renew Energy 2022;183:51–66. https://doi.org/10.1016/j.renene.2021.10.080.
[51] Jabbari B, Jalilnejad E, Ghasemzadeh K, Iulianelli A. Recent progresses in application of membrane bioreactors in production of biohydrogen. Membranes (Basel) 2019;9:1–30. https://doi.org/10.3390/membranes9080100.
[52] Bejan A, Moran MJ. Thermal design and optimization. John Wiley & Sons; 1996.
[53] Zare V. Performance improvement of biomass-fueled closed cycle gas turbine via compressor inlet cooling using absorption refrigeration; thermoeconomic analysis and multi-objective optimization. Energy Convers Manag 2020;215:112946. https://doi.org/10.1016/j.enconman.2020.112946.
[54] Hall SG, Ahmad S, Smith R. Capital cost targets for heat exchanger networks comprising mixed materials of construction, pressure ratings and exchanger types. Comput Chem Eng 1990;14:319–35. https://doi.org/10.1016/0098-1354(90)87069-2.
[55] Baghernejad A, Yaghoubi M. Multi-objective exergoeconomic optimization of an Integrated Solar Combined Cycle System using evolutionary algorithms. Int J Energy Res 2011;35:601–15. doi: 10.1002/er.1715.
[56] Zhao Y, Wang J. Exergoeconomic analysis and optimization of a flash-binary geothermal power system. Appl Energy 2016;179:159–70. https://doi.org/10.1016/j.apenergy.2016.06.108.
[57] Cheddie DF, Murray R. Thermo-economic modeling of a solid oxide fuel cell/gas turbine power plant with semi-direct coupling and anode recycling. Int J Hydrogen Energy 2010;35:11208–15. https://doi.org/10.1016/j.ijhydene.2010.07.082.
[58] Mehr AS, Zare V, Mahmoudi SMS. Standard GAX versus hybrid GAX absorption refrigeration cycle: From the view point of thermoeconomics. Energy Convers Manag 2013;76:68–82. https://doi.org/10.1016/j.enconman.2013.07.016.
[59] Kianfard H, Khalilarya S, Jafarmadar S. Exergy and exergoeconomic evaluation of hydrogen and distilled water production via combination of PEM electrolyzer, RO desalination unit and geothermal driven dual fluid ORC. Energy Convers Manag 2018;177:339–49. https://doi.org/10.1016/j.enconman.2018.09.057.
[60] Shekari Namin A, Rostamzadeh H, Nourani P. Thermodynamic and thermoeconomic analysis of three cascade power plants coupled with RO desalination unit, driven by a salinity-gradient solar pond. Therm Sci Eng Prog 2020;18:100562. https://doi.org/10.1016/j.tsep.2020.100562.
[61] Yu D, Wu J, Wang W, Gu B. Optimal performance of hybrid energy system in the presence of electrical and heat storage systems under uncertainties using stochastic p-robust optimization technique. Sustain Cities Soc 2022;83:103935. https://doi.org/10.1016/j.scs.2022.103935.
[62] Qiao W, Li Z, Liu W, Liu E. Fastest-growing source prediction of US electricity production based on a novel hybrid model using wavelet transform. Int J Energy Res 2022;46:1766–88. doi: 10.1002/er.7293.
[63] Qiao W, Liu W, Liu E. A combination model based on wavelet transform for predicting the difference between monthly natural gas production and consumption of U.S. Energy 2021;235:121216.
[64] Ahmadi P, Dincer I, Rosen MA. Thermodynamic modeling and multi-objective evolutionary-based optimization of a new multigeneration energy system. Energy Convers Manag 2013;76:282–300. https://doi.org/10.1016/j.enconman.2013.07.049.
[65] Hiassat A, Diabat A, Rahwan I. A genetic algorithm approach for location-inventory-routing problem with perishable products. J Manuf Syst 2017;42:93–103. https://doi.org/10.1016/j.jmsy.2016.10.004.
[66] Deb K, Pratap A, Agarwal S, Meyarivan T. A fast and elitist multiobjective genetic algorithm: NSGA-II. IEEE Trans Evol Comput 2002;6:182–97. https://doi.org/10.1109/4235.996017.
[67] Cao Y, Dhahad HA, Togun H, Abdollahi Haghghi M, Anqi AE, Farouk N, et al. Seasonal design and multi-objective optimization of a novel biogas-fueled cogeneration application. Int J Hydrogen Energy 2021;46(42):21822–43.
[68] Wang J, Wang J, Dai Y, Zhao P. Thermodynamic analysis and optimization of a flash-binary geothermal power generation system. Geothermics 2015;55:69–77. https://doi.org/10.1016/j.geothermics.2015.01.012.
[69] Ioroi T, Yasuda K, Siroma Z, Fujiwara N, Miyazaki Y. Thin film electrocatalyst layer for unitized regenerative polymer electrolyte fuel cells. J Power Sources 2002;112:583–7. https://doi.org/10.1016/S0378-7753(02)00466-4.
[70] Yari M, Zarin A, Mahmoudi SMS. Energy and exergy analyses of GAX and GAX hybrid absorption refrigeration cycles. Renew Energy 2011;36:2011–20. https://doi.org/10.1016/j.renene.2011.01.004.
[71] Ramesh kumar A, Udayakumar M. Studies of compressor pressure ratio effect on GAXAC (generator–absorber–exchange absorption compression) cooler. Appl Energy 2008;85(12):1163–72.
[72] Herold KE, Radermacher R, Klein SA. Absorption chillers and heat pumps. CRC Press; 2016.
[73] Kholghi SA, Mahmoudi SMS. Energy and exergy analysis of a modified absorption cycle: A comparative study. Sustainable Energy Technologies and Assessments 2019;32:19–28.
[74] Mohammadzadeh Bina S, Jalilinasrabady S, Fujii H. Exergoeconomic analysis and optimization of single and double flash cycles for Sabalan geothermal power plant. Geothermics 2018;72:74–82. https://doi.org/10.1016/j.geothermics.2017.10.013.
[75] Mosaffa AH, Zareei A. Proposal and thermoeconomic analysis of geothermal flash binary power plants utilizing different types of organic flash cycle. Geothermics 2018;72:47–63. https://doi.org/10.1016/j.geothermics.2017.10.011.
[76] Jing R, Zhu X, Zhu Z, Wang W, Meng C, Shah N, et al. A multi-objective optimization and multi-criteria evaluation integrated framework for distributed energy system optimal planning. Energy Convers Manag 2018;166:445–62.
[77] Cao Y, Dhahad HA, Togun H, Hussen HM, Anqi AE, Farouk N, et al. Feasibility investigation of a novel geothermal-based integrated energy conversion system: Modified specific exergy costing (M-SPECO) method and optimization. Renew Energy 2021;180:1124–47. https://doi.org/10.1016/j.renene.2021.08.075.